Received: 17 April 2021 | Revised: 25 July 2021 | Accepted: 9 August 2021

DOI: 10.1111/bre.12607

RESEARCH ARTICLE

Basin Research EAGE WILEY

Transcontinental retroarc sediment routing controlled by subduction geometry and climate change (Central and Southern Andes, Argentina)

Eduardo Garzanti[1] | **Tomas Capaldi**[2] | **Giovanni Vezzoli**[1] | **Mara Limonta**[1] | **Numa Sosa**[1,3]

[1]Laboratory for Provenance Studies, Department of Earth and Environmental Sciences, Università di Milano-Bicocca, Milano, Italy

[2]Department of Geosciences, University of Nevada, Las Vegas, NV, USA

[3]Centro de Investigaciones Geológicas (CONICET), Universidad Nacional de La Plata, La Plata, Argentina

Correspondence
Eduardo Garzanti, Laboratory for Provenance Studies, Department of Earth and Environmental Sciences, Università di Milano-Bicocca, Milano, Italy.
Email: eduardo.garzanti@unimib.it

Abstract

Central Argentina from the Pampean flat-slab segment to northern Patagonia (27°–41°S) represents a classic example of a broken retroarc basin with strong tectonic and climatic control on fluvial sediment transport. Combined with previous research focused on coastal sediments, this actualistic provenance study uses framework petrography and heavy-mineral data to trace multistep dispersal of volcaniclastic detritus first eastwards across central Argentina for up to ca. 1,500 km and next northwards for another 760 km along the Atlantic coast. Although detritus generated in the Andes is largely derived from mesosilicic volcanic rocks of the cordillera, its compositional signatures reflect different tectono-stratigraphic levels of the orogen uplifted along strike in response to varying subduction geometry as well as different character and crystallization condition of arc magmas through time and space. River sand, thus, changes from feldspatho-litho-quartzose or litho-feldspatho-quartzose in the north, where sedimentary detritus is more common, to mostly quartzo-feldspatho-lithic in the centre and to feldspatho-lithic in the south, where volcanic detritus is dominant. The transparent-heavy-mineral suite changes markedly from amphibole ≫ clinopyroxene > orthopyroxene in the north, to amphibole ≈ clinopyroxene ≈ orthopyroxene in the centre and to orthopyroxene ≥ clinopyroxene ≫ amphibole in the south. In the presently dry climate, fluvial discharge is drastically reduced to the point that even the Desaguadero trunk river has become endorheic and orogenic detritus is dumped in the retroarc basin, reworked by winds and temporarily accumulated in dune fields. During the Quaternary, instead, much larger amounts of water were released by melting of the Cordilleran ice sheet or during pluvial events. The sediment-laden waters of the Desaguadero and Colorado rivers then rushed from the tract of the Andes with greatest topographic and structural elevation, fostering alluvial fans inland and

[Correction added on 10-May-2022, after first online publication: CRUI funding statement has been added.]

flowing in much larger valleys than today towards the Atlantic Ocean. Sand and gravel supply to the coast was high enough not only to promote rapid progradation of large deltaic lobes but also to feed a cell of littoral sediment transport extending as far north as the Río de la Plata estuary.

KEYWORDS

Andean cordillera, Argentina, broken retroarc basin, Desaguadero, Colorado and Negro rivers, drainage network, flat-slab subduction, sedimentary petrology, Sierras Pampeanas

The knight is not free: it moves in an L-shaped manner because it is forbidden to take the straight road."

(Viktor Shklovsky, Knight's Move, 1923)

1 | INTRODUCTION

The horizontal movement of lithospheric plates does not only produce uplift and subsidence, and hence sediment sources and sediment sinks, but also defines and constrains the complex pathways along which detritus moves across continents from source to sink (Audley-Charles et al., 1977; Dickinson, 1988; Potter, 1978). This article investigates transcontinental sediment transfer from an active to a passive continental margin and how variations in subduction style dependent on geological features of the lower plate may influence the retroarc-basin drainage network on the upper overriding plate. The Central and Southern Andes (Figure 1), where latitudinal changes in subduction mode, climate, and continental width have determined a complex evolution of drainage systems along the retroarc-side of the cordillera through time (Potter, 1997), represents a superb training ground in this regard (Capaldi et al., 2020; DeCelles et al., 2011; Horton, 2018).

The Andean cordillera, the largest and longest orogenic belt on Earth, developed in response to eastward subduction of Pacific oceanic lithosphere down the Peru-Chile trench (Figure 2; Ramos, 2009). Subduction angle, generally shallow as typical of east-dipping subduction zones (Aragón et al., 2020; Doglioni, Harabaglia, et al., 1999), is far from constant along strike and geodynamic processes related to the geometry, topographic irregularities, age and thermal state of the subducting plate profoundly influence the interplay among tectonics, climate and sedimentation on the overriding plate at different latitudes (Ramos & Folguera, 2009; Ranero et al., 2006; von Huene et al., 1997).

This sediment-provenance study focuses on central Argentina, where the change from flat-slab subduction between ca. 27°S and 33°S to shallow subduction between 34°S and 40°S (Figure 2) has exerted a fundamental control on the tectonic, magmatic and sedimentary evolution of the retroarc region (Horton et al., 2016; Ramos et al., 2002). In the northern tract drained by the Río Desaguadero, corresponding to the Pampean flat-slab segment, the Andean cordillera reaches the highest elevation, touching 6,962 m above sea level at the summit of Aconcagua, the highest peak on Earth outside the Himalaya-Karakorum Range. Contraction coupled with flexural arching caused by the load of the orogen (Dávila et al., 2007, 2010) triggered the rupture of the retroarc basement and crustal blocks bounded by reverse faults are exposed at altitudes up to 6,097 m a.s.l. in the Sierras Pampeanas (Figure 2). High relief, semiarid climate in the rain shadow of the cordillera and structural partitioning of the broken retroarc basin gave rise to a drainage pattern strongly conditioned by tectonic lineaments and interspersed with dune fields (*médanos*) and saline lakes (Zárate & Tripaldi, 2012), which changed repeatedly in response to changing climatic, magmatic and tectonic regimes through time (Damanti, 1993; Tripaldi & Forman, 2016). Although temporarily stored in

Highlights

- Classic example of broken retroarc basin with strong tectonic and climatic control on sedimentation.
- Sand composition reflects magmatic gap and structural elevation in the Pampean flat-slab segment.
- Volcaniclastic detritus traced E-wards and N-wards for 2,000 km from the Andes to Río de la Plata.
- Stream power, drainage connectivity and sediment fluxes are sharply reduced in present dry climate.
- Retroarc basins, foreland basins and foredeeps are formed by different geodynamic processes.
- Most detritus ends up in the Atlantic Ocean due to low, long-term retroarc-basin storage capacity.

FIGURE 1 F Topography and drainage in central Argentina, with sampling sites (base map from Google Earth™; figure modified from the companion paper Garzanti et al., 2021, where the composition of coastal sands is described in detail). The La Pampa High is interpreted to be the Andean flexural bulge bending the palaeovalley floors ('valles trasversales') that headed eastwards towards the Pampa Deprimida backbulge (Nivière et al., 2013). Rivers: A = Azúl; AE = Agua Escondida; I = Iglesia; P = Pie de Palo. Dune fields: G = Grandes; N = Negro; T = Telteca. F.Z. = Pacific fracture zones. Central Pampean dune field after Zárate and Tripaldi (2012)

sand seas during arid phases or deviated by the uprise of faulted blocks and flexural upwarps (Capaldi et al., 2019; Nivière et al., 2013), large volumes of detritus generated in the highlands have been transferred across the northern Patagonia plateau to the Atlantic Ocean through time.

In this study, we combine framework petrography and heavy-mineral data on sand generated in the Río Desaguadero, Río Colorado and Río Negro catchments to trace provenance and multistep dispersal of volcaniclastic detritus for more than 2,000 km, first southwards and eastwards across central Argentina and next northwards along a littoral cell of sand drift extending as far as the Río de la Plata estuary mouth (Figure 3a; Garzanti et al., 2021). The Argentine coast has long been indicated as a manifest example where transcontinental sediment dispersal leads to large-scale deposition of volcaniclastic detritus with typical magmatic-arc signature onto a passive margin, thus creating a patent mismatch between the tectonic setting of the source and the tectonic setting of the sink (Potter, 1984). Previous studies on compositional signatures and provenance of sediments generated in central Argentina were carried out on Miocene retroarc-basin deposits (e.g. Pinto et al., 2018) and on modern sediments of Río Colorado (Blasi, 1991; Blasi & Manassero, 1990), Río Desaguadero (Capaldi et al., 2017, 2019), dune fields (Tripaldi et al., 2010) and beaches (Potter, 1994; Teruggi et al., 1959, 1964).

The main goal of this actualistic provenance study is to build on our present knowledge of complex sedimentary systems associated with orogenic belts, thus increasing the intelligence needed to unravel the interplay of processes controlling landscape evolution and decrypt the stratigraphic archive. Research on modern sediments specifically aimed at improving our understanding of the relationships between the geology of orogenic source areas and the petrographic and mineralogical signatures of detritus derived from them represents an essential step to interpret ancient sandstone suites and reconstruct the history of adjacent orogenic belts. In the final part of this article, we shall broaden our view to contrast what we believe to be

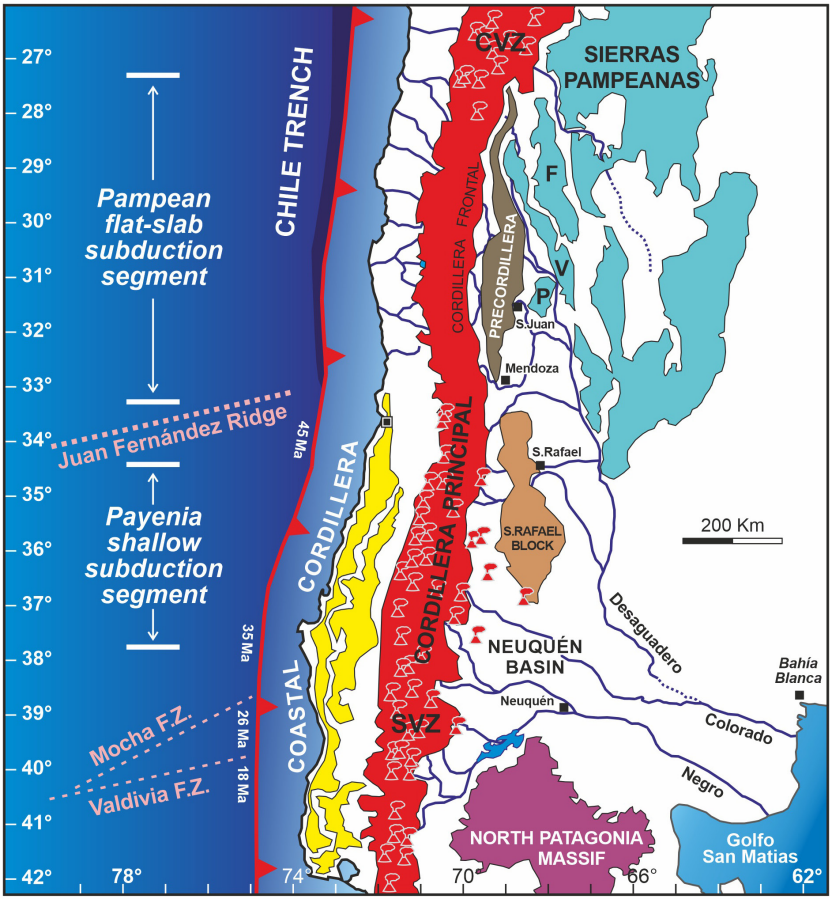

FIGURE 2 Main tectonic domains (redrawn after Ramos & Folguera, 2005, 2009). Distribution of volcanism in the central (CVZ) and southern (SVZ) active volcanic zones separated by the Pampean flat-slab segment, fracture zones and age of subduction of Pacific lithosphere after Stern (2004) and Geological Map of South America (2019). Sierras Pampeanas: F = Famatina; P = Pie de Palo; V = Valle Fértil

three fundamentally distinct types of sedimentary basins associated with three different types of orogenic belts, archetypes of which are considered the Andes, the Himalaya and the Apennines. These three basin types are formed in geodynamic settings characterized by a remarkably different system of applied forces, leading to radically different subsidence magnitude and hence radically different sediment storage versus export capacity, drainage networks and compositional signatures of terrigenous sediments.

2 | RETROARC-BASIN LANDSCAPES AND RIVER SYSTEMS

The studied Desaguadero, Colorado and Negro river catchments jointly cover an area of 530,000 km^2 (a fifth of the entire Argentina; Figure 1). These rivers have their headwaters in the high-relief Andean cordillera, which receives limited amounts of rainfall especially in the north, and cross the wide semiarid Patagonian plateau covered by grassy steppe vegetation to reach the Atlantic Ocean. Before being disconnected in the presently dry climatic condition, the Desaguadero and Colorado rivers joined ca. 300 km upstream of the mouth and their catchment covered an area of 400,000 km^2 spanning almost thirteen degrees of latitude (Figure 1).

2.1 | Climate and landscape

The high Andean cordillera represents a barrier to the strong prevailing westerlies, causing orographically enhanced rainfall on the western Chilean side (Figure 3a). Annual precipitation exceeds 800 mm in a narrow strip along the Southern Andes and rapidly decreases northwards and eastwards across the Argentine retroarc region that remains in the rain shadow. The southeast trade-wind circulation associated with the Atlantic subtropical anticyclone, however, carries abundant moisture to the Argentine Pampas east of the Andes (Figure 3b). Climatic conditions, thus, vary from temperate humid to sub-humid in the cordillera (mean temperature 6–8°C) to the semiarid northern Patagonian plateau, where annual rainfall is ca. 200 mm and mean temperature 14–16°C (Brunet et al., 2005).

The dry northernmost part of the study area is drained by the endorheic Río Abaucán (Figure 1), which loses its waters in a salty semi-desert (*Desague del Río Salado*). In the upper catchment of Río Desaguadero, a series of vegetated and mostly stabilized dune fields (*médanos*), grown and sculpted by interplaying fluvial and aeolian processes, represent the remnants of a wide late Pleistocene Pampean Sand Sea (Figure 3b; Iriondo, 1999). The Colorado and Negro drainage basins straddle the boundary between

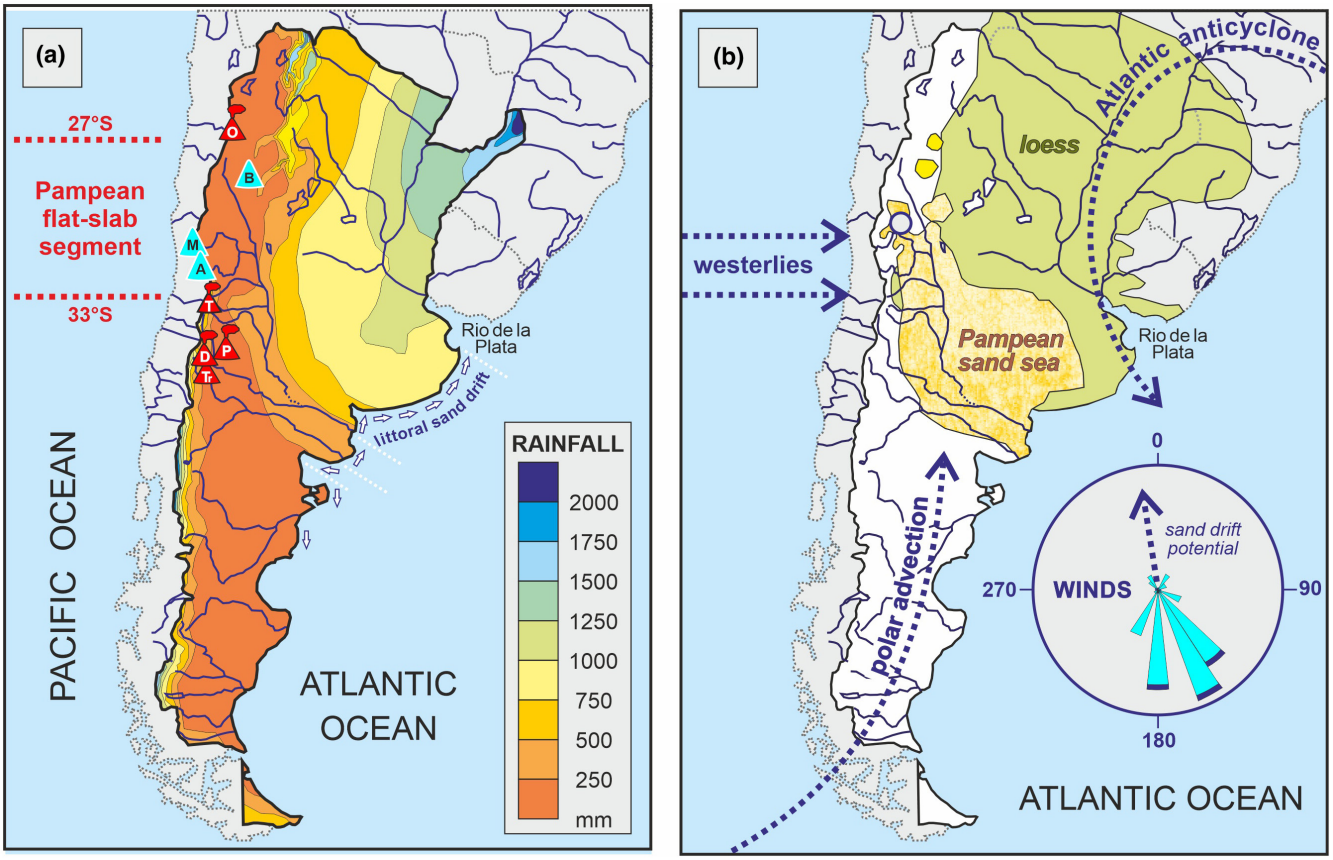

FIGURE 3 Climate and landscapes of Argentina. (a) Rainfall map (after Bianchi & Cravero, 2010). Longshore sand transport after Garzanti et al. (2021). Highest peaks in the cordillera (A = Cerro Aconocagua: M = Cerro Mercedario) and in the Sierras Pampeanas (B = Cerro General Belgrano) coincide with the Pampean flat-segment and magmatic gap between the Central Volcanic Zone (O = Ojos del Salado) and northern Southern Volcanic Zone (D = Domuyo; P = Payún Matrú; Tr = Tromen; T = Tupungato). (b) Aeolian deposits and wind regimes (after Tripaldi & Forman, 2007, 2016). Wind rose for 1995–2004 near San Juan (grey circle)

subtropical summer and mid-latitude winter rains. Landscapes change in cold semiarid Patagonia to the south, where hundreds of glacial lakes occur along the Andean foothills. Lake Nahuel Huapi (area 557 km^2, depth ≤157 m), feeding Río Limay, is an oligotrophic proglacial lake with clear waters (Figure 1; Markert et al., 1997).

2.2 | Río Desaguadero

Río Desaguadero —named Bermejo upstream of the Río San Juan confluence, Salado upstream of the Río Atuel confluence, next Chadileuvú (in Mapuche language *chadi*, salt; *leuvú*, river), and finally Curacó — has a drainage area of ca. 300,000 km^2 and flows southwards for almost 1,500 km along the Andean retroarc basin, characterized by broad floodplains and ephemeral salty lagoons. The river drains the tract of the Central Andes corresponding to the Pampean flat-slab subduction segment (Figure 2), where Palaeozoic to Miocene rocks have been tectonically uplifted to nearly 7,000 m a.s.l. in the Aconcagua massif (Figure 3; Farías et al., 2008; Ramos & Folguera, 2009). Tributaries carrying detritus from the Cordillera Principal, Cordillera Frontal, Precordillera and Sierras Pampeanas generate alluvial megafans at entry points into the retroarc basin, where wind reworking in arid climatic conditions has promoted the growth of dune fields (Tripaldi & Forman, 2007).

Río Bermejo, the upstream branch of Río Desaguadero, flows along a Neogene strike-slip fault across the western Sierras Pampeanas (Introcaso & Ruiz, 2001), which reach above 6,000 m a.s.l. in the Sierra de Famatina (*F* in Figure 2; *B* in Figure 3). Detritus is, thus, derived not only from the Andes but also from basement rocks exhumed in the Sierra Valle Fértil and Sierra Pie de Palo uplifts (*V* and *P* in Figure 2; Ramos et al., 2002). The Río San Juan, sourced from the Cordillera de la Ramada and Mercedario massif, drains the Cordillera Frontal and the Precordillera fold-thrust belt. The Río Mendoza is sourced from the Aconcagua massif in the Cordillera Principal (A

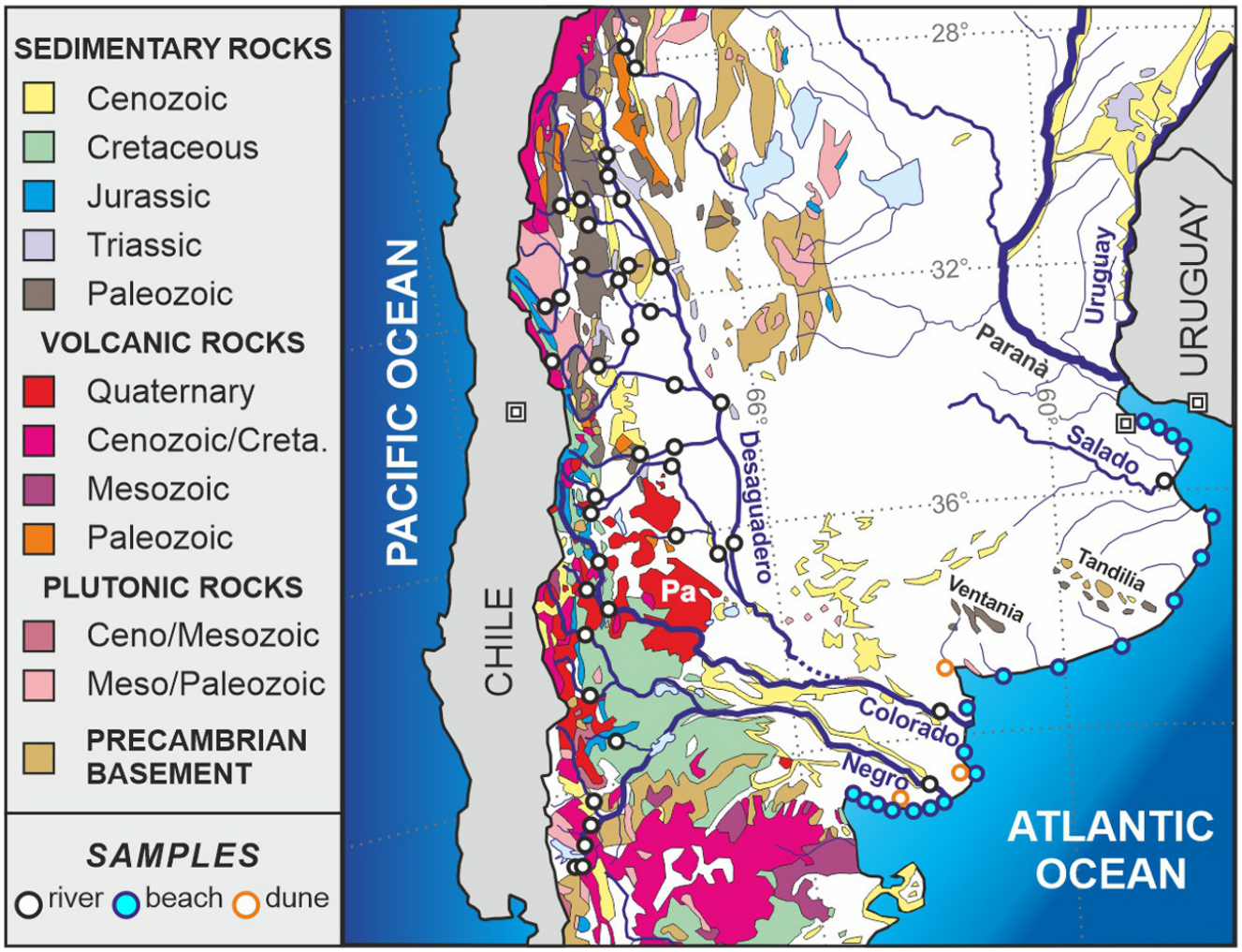

FIGURE 4 F Geological map of central Argentina (after Schenk et al., 1999 and Geological Map of South America, 2019) with sampling sites (the composition of coastal sands is described in detail in the companion paper Garzanti et al., 2021). Pa = Payenia volcanic province

in Figure 3) and cuts across the Cordillera Frontal and the southern tip of the Precordillera to reach the retroarc basin, where it flows northwards along the western border of the Médanos Telteca to join Río San Juan south of the Médanos Grandes (Capaldi et al., 2019).

2.3 | Río Colorado

Río Colorado (in Mapuche language *Colú Leuvú*: *colo/coli*, brownish/coloured) owes its name to its brownish, sediment-laden waters. Formed by the confluence between the Río Grande and Río Barrancas, the river is ca. 1,100 km-long with a basin area of ca. 70,000 km^2. Sourced in the Cordillera Principal, the river drains the northern Neuquén Basin and basalts of the Quaternary Payenia volcanic province (Pa in Figure 4; Ramos & Folguera, 2011). In this region, basaltic lavas were emplaced as far as 500–600 km away from the trench also during the late Miocene, a period of inferred shallow subduction and eastward arc migration (Litvak et al., 2015; Stern, 2004). Downstream, the river crosses the arid northern Patagonia plateau and the southern Pampa and is estimated to deliver 4–4.5 km^3 of water, ca. 7·10^6 tons of suspended solids, and ca. 3·10^6 tons of dissolved solids to the Atlantic Ocean (Latrubesse & Restrepo, 2014; Milliman & Farnsworth, 2011, p. 209). Discharge fuelled by melting of mountain snow reaches maximum in October and continues during the rainy summer.

2.4 | Río Negro

The ca. 1,200-km-long Río Negro (in Mapuche language *Curú Leuvú*: *curú*, black), formed by the confluence between Río Limay and Río Neuquén, is the largest river of

Patagonia. Sourced in the Cordillera Principal, the Río Negro drains the Agrio fold-thrust belt and the southern Neuquén basin, where an Upper Triassic to Paleogene continental and marine sedimentary succession is exposed (Howell et al., 2005; Valcarce et al., 2006; Zapata & Folguera, 2005). The drainage basin (ca. 130,000 km^2), situated between 36°S and 42°S, is characterized by a strong climatic gradient from the Andean slopes – receiving up to 3,000 mm of annual rainfall locally (Lago Frías) – to Neuquén (500 mm) and the river mouth (100–200 mm). Annual water discharge (23 km^3 for Río Limay and 9 km^3 for Río Neuquén; Bonetto & Wais, 2006) has two maxima, fed from melting of mountain ice and snow in spring and by heavy rains in winter (May to August). The discharge of Río Limay (62,000 km^2), the emissary of Lake Nahuel Huapi (*limay*, clear water; *nahuel*, jaguar; *huapi*, island), is regulated naturally upstream by glacial lakes and artificially downstream by a sequence of five big dams closed between 1973 and 1999. The Río Neuquén (ca. 40,000 km^2) gave rise to sudden floods causing serious economic losses. For both flood-control and hydropower generation, a series of dams (Cerros Colorados Complex) were, thus, built between 1969 and 1980 on the lower Neuquén valley and excess flow during flood can now be diverted *via* an artificial channel towards the natural depressed area of Lago Pellegrini. Río Negro is estimated to deliver 13–18·10^6 tons of suspended solids and ca. 5·10^6 tons of dissolved solids to the Atlantic Ocean (Latrubesse & Restrepo, 2014; Milliman & Farnsworth, 2011, p. 209).

2.5 | The Atlantic coast

The Argentine continental shelf is one of the largest and smoothest shelves in the world (average width 400 km). This passive continental margin developed during the initial opening of the South Atlantic and is characterized by several failed rifts orthogonal to the continent-ocean boundary (e.g. Colorado basin; Franke et al., 2006) formed by NE–SW extension in the late Mesozoic during clockwise rotation away from Africa (Richetti et al., 2018).

The ca. 1,500-km-long Atlantic coast from Golfo San Matias to Río de la Plata has no major river outlet besides the Negro and Colorado mouths, which are only 190 km apart. The few other small rivers and creeks supply negligible amounts of sediment, whereas contribution from cliff erosion is significant (Isla & Cortizo, 2014). Dominantly siliciclastic sedimentation was profoundly affected by late Pleistocene to Holocene climatic and eustatic changes, which determined large variations of detrital supply with phases of deltaic growth followed by reworking by waves and tides (Ponce et al., 2011). Sediment fluxes from the Andes have been progressively reduced as an effect of drying climate, and eventually in the last century by flood regulation and construction of major dams since 1969 in the Río Negro catchment and by closure of the Casa de Piedra Dam on Río Colorado in 1996 (Piccolo & Perillo, 1999).

The Río Negro mouth is a mesotidal inlet with an asymmetric ebb tidal delta, indicating net northward longshore sand transport (del Rio et al., 1991). Littoral sand drift fuelled by swell waves from the SW feeds stable to rapidly prograding beaches north of the mouth. Here, backshore dunes migrate north-eastwards under the prevalent effect of strong winds from the south-west (Cortizo & Isla, 2012; Vergara Dal Pont et al., 2017).

The coast to the north includes the deltaic lobe of Río Colorado, prograding slowly and deflected northwards by longshore currents, together with several tidal channels, salt marshes, and tidal flats representing the remnants of a ca. 200-km-wide deltaic complex formed by Río Colorado in the late Pleistocene–early Holocene (Spalletti & Isla, 2003). The ca. 660-km-long mesotidal to microtidal coast of the Buenos Aires Province farther north includes wide sandy beaches and backshore dunes (Isla et al., 2001) with coastal stretches undergoing erosion especially in anthropized areas (Isla et al., 2018). Swells and storm waves impacting obliquely onto the coast mainly from the south promote a steady northward littoral sand drift in winter and spring, with partial inversion in summer months when northerly winds predominate (Isla, 2014). Northward littoral sand drift was most active in the late Pleistocene–early Holocene, when alternating waxing and waning of glaciers and more humid stages provided suitable conditions for the efficient fluvial transfer of much larger volumes of volcaniclastic detritus from the Andes to the Atlantic Ocean than today (Spalletti & Isla, 2003; Zárate & Blasi, 1993).

3 | GEOLOGICAL FRAMEWORK

The Andean cordillera has undergone a complex tectonic evolution, traditionally subdivided into five main orogenic cycles, the latest Neoproterozoic Pampean stage (555–515 Ma), the Cambro-Ordovician Famatinian stage (495–460 Ma), the Carboniferous to Middle Triassic Gondwanian stage, the Jurassic–Cretaceous Patagonide stage and the Cenozoic Andean stage (Charrier et al., 2015; Ramos, 1988). The southern Central Andes (Pampean segment) and northern Southern Andes (Payenia to northern Patagonia segment) exhibit significant along strike variation in subduction angle, tectonic shortening, magmatism and exposed geological units (Figure 4).

3.1 | Pampean segment (27°–33°S)

The modern Pampean segment of the Nazca-South America plate boundary is characterized by very shallow subduction, a ca. 600-km-long gap in active volcanism, and basement uplifts of the Sierras Pampeanas (Alvarado et al., 2009; Barazangi & Isacks, 1976; Jordan et al., 1983). These basement blocks occupy an area larger than the orogen, extending inland towards the Río de la Plata Craton for up to 430 km. Flat subduction may have started when the Juan Fernández Ridge in the Nazca Plate reached the Chilean trench, and propagated southwards during the Miocene. The corresponding diachronous uplift of the Sierras Pampeanas initiated in the latest Miocene at 27°S and continued through the Pliocene at 33°S (Ramos et al., 2002). The Pampean flat-slab segment of the Andes comprises a Jurassic–Cenozoic magmatic arc (Cordillera Principal), Carboniferous–Triassic basement uplifts (Cordillera Frontal), a thin-skinned, fold-thrust belt (Precordillera), an adjacent broken retroarc basin (Bermejo Basin) and basement-cored block uplifts (Sierras Pampeanas; Figure 2).

The Andean magmatic arc, generated by east-dipping subduction of Paleo-Pacific plates, consists of N/S-trending belts of mostly granite/granodiorite intrusions and andesite lava flows. These belts show a systematic eastward decrease in age, from Jurassic (200–165 Ma) and Cretaceous (130–90 Ma) along the Chilean coast, to Palaeocene–Eocene (67–38 Ma) and Oligocene–Miocene (27–18 Ma) along the western flank of the Cordillera Principal, and finally Neogene (17–2 Ma) volcanic rocks in the eastern Cordillera Principal, Cordillera Frontal and retroarc region (Haschke et al., 2006; Jones et al., 2016; Kay et al., 1991; Parada et al., 1988, 1999).

Carboniferous–Triassic igneous rocks form much of the Cordillera Frontal, with the Choiyoi igneous complex spanning the Cordillera Principal along the Chile–Argentina border and flanking regions to the west and east including the retroarc region (Kleiman & Japas, 2009; Ramos et al., 2004). Batholith emplacement in the northern Cordillera Frontal involved diverse successive phases of Carboniferous to Triassic orogenic and post-orogenic magmatism (Hervé et al., 2014; Sato et al., 2015). Late Carboniferous to Early Permian magmatism was synchronous with growth of the NW-trending Gondwanide orogenic belt (Giambiagi et al., 2014; Hervé et al., 2014; Nelson & Cottle, 2019). After the cessation of Gondwanide shortening and crustal thickening, the emplacement of calc-alkaline to alkaline bimodal intrusive suites and exceptionally thick (>5 to 10 km) ignimbrites of the Choiyoi Group (ca. 280–248 Ma) is consistent with crustal melting and possible post-orogenic disruption during the earliest stages of Gondwana breakup (Kleiman & Japas, 2009; Mpodozis & Kay, 1992; Sato et al., 2015).

The Precordillera is an east-directed, fold-thrust belt involving a Palaeozoic marine clastic and carbonate succession (Allmendinger & Judge, 2014). The Cambrian–Ordovician carbonate platform is overlain by Upper Ordovician–Devonian clastic rocks in eastern and central thrust sheets, passing to slope and deep-marine facies in western thrust sheets. Carboniferous–Permian marine to non-marine strata follow. The Silurian–Devonian sediments are derived from the Cuyania basement and Famatinian arc, whereas Carboniferous–Permian sediments are dominated by Famatinian and Pampean arc material with some input from a nascent Carboniferous arc (Capaldi et al., 2017). Over 100 km of E–W shortening was accommodated by imbricate thrusting above a ca. 12-km-deep décollement (Cristallini & Ramos, 2000; Fosdick et al., 2015; von Gosen, 1992).

The proximal Bermejo retroarc basin flanking the Precordillera contains a thick, principally Miocene succession of fluvial and alluvial-fan deposits (Capaldi et al., 2020; Johnson et al., 1986; Jordan et al., 1993, 2001; Reynolds et al., 1990). Active megafans were fed by large catchment areas (>10,000 km^2) with focused entry points into the retroarc basin (Damanti, 1993).

The western Sierras Pampeanas (i.e. Pie de Palo, Umango and Maz-Espinal) consist of Mesoproterozoic mafic-ultramafic rocks representative of the Grenville-aged basement of the Cuyania-terrane and lower Palaeozoic metasedimentary rocks (Rapela et al., 2010, 2016). Uppermost Ediacaran to Devonian igneous and metamorphic rocks are exposed across the eastern Sierras Pampeanas (Valle Fértil and Famatina), including the roots of the Cambro–Ordovician Famatinian arc and of the Ediacaran–Cambrian Pampean arc (Sierra de Cordoba) (Bahlburg et al., 2009; Ramos et al., 1986). The Precambrian to Ordovician history included accretion of Laurentian terranes (e.g. Cuyania) to the Gondwana margin, followed by accretion of the Chilenia terrane (Martin et al., 2020; Ramos et al., 1984; Thomas et al., 2015). Isolated granitic plutons of Devonian age occurring across the region are interpreted to have been emplaced during extension (Dahlquist et al., 2013; Moreno et al., 2020).

3.2 | Payenia to northern Patagonia segment (34°–42°S)

The northern Southern Andes are characterized by the active Southern Volcanic Zone, broad and low-relief retroarc-basin uplifts and higher dip of the subducting Nazca slab, which progressively increases from ca. 30° in the Payenia segment to ca. 55° in northern Patagonia (Folguera & Ramos, 2011; Horton et al., 2016). In this region of Argentina, the Andes consist of a magmatic

arc (Cordillera Principal) with a thin-skinned belt locally involving basement (Malargüe, Agrio, and North Patagonian fold-thrust belts). The eastern retroarc basin (Neuquén Basin) is partitioned by basement uplifts (San Rafael Block and North Patagonian Massif) and hosts large Neogene to recent igneous provinces (Payenia and Somuncurá volcanic fields).

The Southern Volcanic Zone is emplaced over exhumed Middle Jurassic to upper Miocene magmatic rocks. The Andean drainage divide north of 38°S is formed by upper Oligocene to upper Miocene volcanic and volcaniclastic rocks preserved in extensional within-arc basins (Charrier et al., 2002; Mackaman-Lofland et al., 2019). The northern Patagonia Andean magmatic arc includes numerous NW-trending belts of plutonic suites and volcanic equivalents, including the Lower Jurassic Subcordilleran Belt (ca. 185–181 Ma) and the Cretaceous to Cenozoic North Patagonian Batholith (ca. 173–5 Ma; Aragón et al., 2011; Pankhurst et al., 1999; Rapela et al., 2005). The eastward advance of the Andean magmatic arc in northern Patagonia at ca. 90–70 Ma and subsequent cessation during ca. 70–55 Ma reflected a transient slab-shallowing event (Butler et al., 2020; Folguera & Ramos, 2011; Gianni et al., 2018).

The Malargüe and Agrio fold-thrust belts involve a complex combination of detached thin-skinned and basement-involved structures that commonly reactivated Mesozoic normal faults, with shortening estimated as 15–45 km (Folguera et al., 2015; Fuentes et al., 2016; Giambiagi et al., 2012). The North Patagonian fold-thrust belt deforms Jurassic–Cretaceous plutonic rocks and Jurassic–Neogene volcanic rocks along basement-involved structures indicating <10 km of E/W shortening (Ramos et al., 2014).

The triangular Neuquén Basin contains a 5–7-km-thick succession of Upper Triassic to Neogene quartzo-feldspatho-lithic to litho-feldspatho-quartzose sandstones, black shales and minor carbonates and evaporites tapering eastwards onto the San Rafael Block to the north and onto the North Patagonian Massif to the south (Di Giulio et al., 2012, 2017; Eppinger & Rosenfeld, 1996; Howell et al., 2005). The stratigraphic succession records initial Mesozoic extension and thermal subsidence followed by flexural subsidence of the Upper Cretaceous–Cenozoic retroarc basin interrupted by a prolonged mid-Eocene to early Miocene (ca. 40–20 Ma) depositional hiatus (Horton et al., 2016).

The San Rafael Block is a broad, east-verging basement-involved uplift consisting of Mesoproterozoic metamorphic rocks and tightly folded Palaeozoic metasedimentary rocks intruded and unconformably overlain by Permian to Triassic granitoids and volcanic rocks of the Choiyoi Group (Kleiman & Japas, 2009; Ramos & Kay, 2006). The pre-Carboniferous stratigraphic units, preserving structures related to the Gondwanide orogeny, have been associated with the Cuyania terrane and Precordillera to the north (Cingolani & Ramos, 2017). Triassic rift basins were inverted during the Andean orogeny (Ramos et al., 2004).

Overlying the San Rafael Block are the Pliocene to Holocene basaltic flows and cinder cones of the Payenia volcanic province (Ramos & Folguera, 2011). Magmatism may have been triggered by a short-lived episode of flat-slab (and plume?) subduction followed by injection of hot asthenosphere during re-steepening of the subducting Nazca Plate (Folguera et al., 2009; Gianni et al., 2017; Kay et al., 2006). The North Patagonian Massif consists of Paleozoic–Mesozoic metamorphic and igneous rocks capped by a voluminous Jurassic rhyolitic ignimbrite associated with the Chon Aike province (Pankhurst & Rapela, 1995). The Somuncurá volcanic province in the eastern part of the North Patagonian Massif records extensive mafic magmatism peaking between ca. 27 and 22 Ma (Kay et al., 2007).

4 | SAMPLING AND ANALYTICAL METHODS

In this study, we have analysed 40 modern sand samples collected between 2014 and 2018 on active bars of the Abaucán, Desaguadero, Colorado and Negro rivers, and of their tributaries and sub-tributaries in Argentina from Tinogasta (ca. 28°S) to San Carlos de Bariloche (ca. 41°S). Another 25 modern sand samples from beaches, rivers and aeolian dunes collected along the Argentine coast between Río de la Plata (ca. 35°S) and Golfo San Matias (ca. 41°S) were studied with the same methodological approach and described in Garzanti et al. (2021). Full information on all sampling sites is provided in Table S1 and in the Google Earth file *ArgenRetroarc.kmz*.

An aliquot of each sand sample was impregnated with araldite epoxy and cut into a standard thin section stained with alizarine red to distinguish dolomite and calcite. Petrographic analyses were carried out by counting 450 points on each thin section following the Gazzi-Dickinson method (Ingersoll et al., 1984). Sand classification was based on the relative abundance of the three main framework components quartz (Q), feldspars (F) and lithic fragments (L), considered if exceeding 10%QFL. According to standard use, the less abundant component goes first, the more abundant last (e.g. a sand is named quartzo-litho-feldspathic if F > L > Q > 10%QFL). Fifteen fields are, thus, defined in the QFL plot; if quartz, feldspar and lithic fragments are all present in subequal proportions, (i.e. ≥30%QFL), then a Q ≈ F ≈ L field is also considered. (Garzanti, 2019, p. 551). Rock fragments were classified

according to protolith composition and metamorphic rank (Garzanti & Vezzoli, 2003).

Heavy-mineral analyses were carried out on the 15–500 μm class obtained by wet sieving. From a split aliquot of each bulk sample, the dense mineral fraction was separated by centrifuging in Na-metatungstate (density 2.90 g/cm^3) and recovered by partial freezing with liquid nitrogen. In order to obtain correct volume percentages of diverse species, ≥200 transparent heavy minerals were point-counted at suitable regular spacing on each grain mount (Garzanti & Andò, 2019).

Transparent heavy-mineral assemblages are called 'tHM suites' for brevity throughout the text. Rock fragments, iron oxides, soil clasts, phyllosilicates and carbonates were not considered as integral part of the tHM suite. According to the concentration of transparent heavy minerals (tHMC index of Garzanti & Andò, 2007), tHM suites are described as 'poor' (tHMC <1), 'moderately poor' (1 ≤ tHMC < 2), 'moderately rich' (2 ≤ tHMC < 5), 'rich' (5 ≤ tHMC < 10) or 'very rich' (10 ≤ tHMC < 20).

The ZTR index (sum of zircon, tourmaline and rutile over total tHM; Hubert, 1962) expresses the durability of the tHM suite through multiple sedimentary cycles (Garzanti, 2017). The Amphibole Colour Index (ACI) varies from 0 in detritus from low-grade metamorphic rocks yielding exclusively blue-green amphibole to 100 in detritus from granulite-facies or volcanic rocks yielding exclusively brown amphibole and oxyhornblende. The ACI resulted to be particularly useful to discriminate between magmatic amphiboles derived from the Andean cordillera (brown titanian pargasite and magnesio-hornblende; Deruelle, 1982; Pinto et al., 2018) from blue-green amphiboles shed by the Sierras Pampeanas.

Other parameters used are the P/F (plagioclase/total feldspar) ratio, which increases with increasing percentage of volcanic supply, and the Vm/V (mafic+intermediate volcanic/total volcanic rock fragments) and Cpx/Px (clinopyroxene/total pyroxene) ratios, which decrease with increasing silica content of volcanic source rocks. Significant detrital components are listed in order of abundance (high to low) throughout the text. The complete petrographic and heavy-mineral datasets are provided in Tables S2 and S3.

5 | SAND PETROGRAPHY AND HEAVY MINERALS

In this section, we illustrate first the main mineralogical signatures of sand generated in the Desaguadero, Colorado and Negro river catchments (Figure 5) and next briefly summarize sand composition in beaches and aeolian dunes along the Atlantic coast (Table 1).

5.1 | Río Desaguadero and tributaries

Sand composition changes progressively southwards along the Desaguadero mainstem (Figure 6a), from litho-feldspatho-quartzose in Río Bermejo upstream (Figure 5d) to feldspatho-litho-quartzose downstream of the Tunuyán confluence and eventually quartzo-feldspatho-lithic volcaniclastic upstream of the Atuel confluence (Figure 5i). Microlitic volcanic lithics prevail over felsitic and lathwork types; sedimentary and metasedimentary lithics are subordinate and decrease downstream (Figure 6b). Plagioclase prevails over K-feldspar (Figure 6c). Celestite grains or mud clasts frequently occur and are locally abundant in Desaguadero and Atuel river sand, respectively. The moderately poor to moderately rich tHM suite mainly contains amphibole with garnet and clinopyroxene in Río Bermejo and subequal amounts of augitic clinopyroxene, orthopyroxene (hypersthene) and amphibole (green-brown hornblende and oxyhornblende with very minor blue-green hornblende), with minor epidote, garnet and zircon downstream (Figure 6d,e).

Most Desaguadero tributaries carry quartzo-feldspatho-lithic sand with plagioclase ≫K-feldspar, lathwork, microlitic and felsitic volcanic lithics. Quartz content is highest in Abaucán and Bermejo sand in the north (Figure 5d), intermediate in San Juan and Mendoza sand in the centre (Figure 5e) and lowest in Atuel sand in the south (Figure 5h). Sedimentary and low-rank metasedimentary rock fragments also decrease southwards. Commonly perthitic K-feldspar, biotite and mainly felsic (quartz-feldspar) to intermediate (plagioclase-hornblende) igneous/metaigneous rock fragments are most common in Río Mendoza sand at the mountain front. Carbonate rock fragments occur but are never abundant. Shale, slate and phyllite rock fragments are most common in Río Jáchal sand. Quartz tends to slightly increase downstream Río San Juan and Río Mendoza, but otherwise no clear systematic compositional trend is displayed from west to east across the cordillera.

Heavy-mineral assemblages are more varied and show clearer trends from north to south. In the north, mainly moderately rich tHM suites are amphibole-rich and orthopyroxene-poor, with clinopyroxene, locally common garnet, subordinate epidote, zircon, apatite, minor titanite and rare staurolite, kyanite or sillimanite. ZTR indices are slightly higher and ACI indices lower than in the south; olivine was never detected. Amphibole dominates the moderately rich tHM suite of the Río Iglesia, one headwater branch of the Río Jáchal, whereas the rich tHM suite of Río Jáchal sand downstream of the Cuesta del Viento Dam is clinopyroxene-dominated. The moderately poor tHM suite of San Juan and Mendoza sands mostly contains clinopyroxene and amphibole, with minor epidote

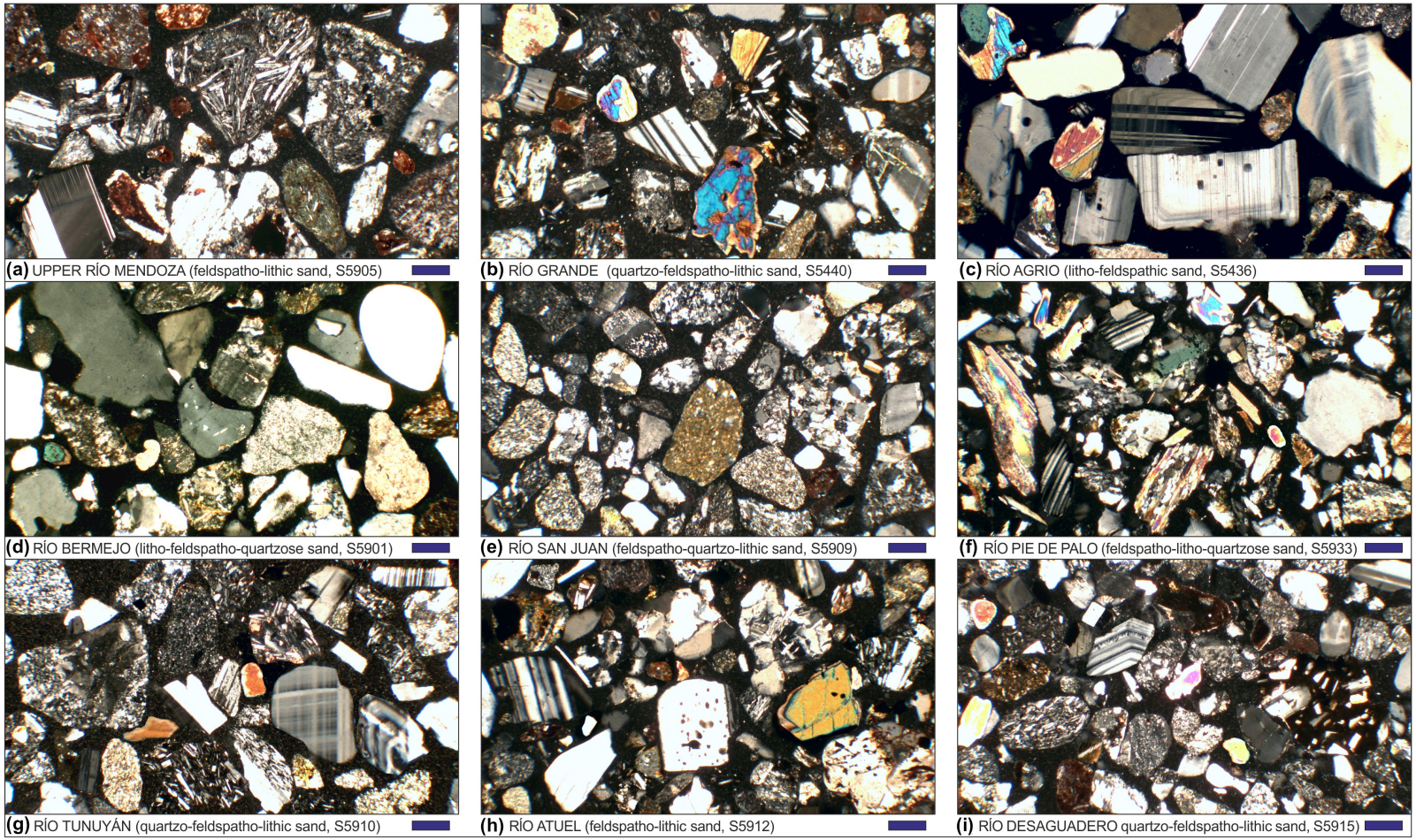

FIGURE 5 Petrography of river sands. Dominantly volcanic sources: (a) Plagioclase and microlitic to felsitic volcanic rock fragments shed from the Cordillera Principal (Aconcagua massif; Río Desaguadero catchment). (b) Plagioclase, pyroxene and mainly microlitic volcanic rocks fragments derived from the Cordillera Principal and Payenia volcanic province (Río Colorado catchment). (c) Dominant plagioclase showing oscillatory zoning from the Cordillera Principal (Río Negro catchment). Additional sedimentary sources: (d) Recycled rounded quartz and carbonate grains (right of photo); (e) arenaceous and siltstone grains (centre of photo). Dominantly metamorphic sources: (f) quartz, feldspars and high-rank metapelite and metapsammite grains from the Sierras Pampeanas. Rivers in the retroarc basin: (g) zoned plagioclase, volcanic rock fragments and siltstone/metasiltstone grains. (h) typical low-quartz volcaniclastic Andean sand. (i) Plagioclase with oscillatory zoning, microlitic and glassy volcanic rock fragments. All photos with crossed polars; blue bar for scale = 100 μm

TABLE 1 Framework petrography and transparent-heavy-mineral suites

River	Sample	Q	F	Lvm	Lsm	Lm[h]		P/F	Vm/V	tHMC	ZTR	Ep	Grt	Amp	Cpx	Opx	Ol	Ap	&tHM		ACI	Cpx/Px
Pie de Palo	1	52	20	2	3	23	100.0	78	n.d.	15.8	1	6	34	57	0	0	0	0	2	100.0	11	n.d.
Abaucán	2	46	23	18	12	1	100.0	76	71	2.8	5	10	3	39	30	10	0	2	1	100.0	64	72
Desaguadero catchment																						
Upper Bermejo	2	41	31	14	12	1	100.0	87	75	2.2	2	10	7	64	9	3	0	3	1	100.0	58	77
Lower Bermejo	2	57	25	10	8	1	100.0	82	51	2.6	7	8	21	44	13	1	0	2	2	100.0	42	90
Jáchal	1	11	21	26	40	2	100.0	99	92	8.4	0	0	0	6	93	1	0	0	0	100.0	64	98
Jáchal tributaries	2	30	33	20	17	1	100.0	88	74	2.6	4	6	3	57	24	2	0	3	1	100.0	74	80
Upper San Juan	4	20	28	40	12	0	100.0	87	62	1.4	2	5	1	35	53	3	0	1	0	100.0	82	95
Mendoza	3	13	39	37	9	1	100.0	84	67	1.7	4	7	1	41	35	8	0.1	4	0.3	100.0	74	77
Lower San Juan	1	30	33	30	7	1	100.0	82	71	1.9	2	4	3	45	24	20	0	1	0	100.0	72	54
Upper Desaguadero	1	38	28	28	5	1	100.0	62	37	1.5	4	6	3	26	33	26	1	1	0.5	100.0	76	56
Tunuyán	1	17	31	42	8	1	100.0	82	86	2.1	0.5	0.5	1	38	26	33	0.5	0	0.5	100.0	80	44
Diamante	2	11	36	44	7	1	100.0	97	82	8.8	0.7	0.2	1	17	31	45	4	0.5	0	100.0	81	42
Atuel	5	10	35	47	8	0	100.0	95	88	5.8	0.1	3	2	10	43	40	2	0.5	0	100.0	84	52
Lower Desaguadero	1	21	35	36	6	1	100.0	94	71	3.9	2	6	3	27	28	32	0	1	0.5	100.0	79	47
Colorado catchment																						
Grande	1	13	39	42	6	0	100.0	95	84	5.7	0.5	0.5	0.5	20	45	31	2	0.5	0	100.0	89	59
Barrancas	1	10	43	39	9	0	100.0	95	93	4.5	2	2	0.5	6	55	32	0.5	1	0	100.0	90	63
Upper Colorado	1	12	34	44	10	0	100.0	95	87	6.6	0.5	0	2	19	34	33	11	1	0	100.0	93	51
Lower Colorado	1	24	32	40	4	0	100.0	85	87	4.4	0.9	1	5	7	45	38	3	0	0	100.0	81	54
Negro catchment																						
Nahuel Huapi	2	14	33	47	3	4	100.0	96	95	5.5	0.5	1	0.2	5	22	67	3	0.2	0	100.0	48	25
Limay	2	9	34	56	1	1	100.0	95	99	3.9	0.5	2	0	4	30	61	3	0	0	100.0	39	33
Collon Cura	1	10	33	56	1	1	100.0	98	97	6.8	0	8	0	6	36	45	4	0.5	0	100.0	59	44
Picun Leuvú	1	34	31	27	7	1	100.0	77	76	1.3	5	0.5	0.5	5	36	37	15	1	0.5	100.0	67	49
Agrio	1	6	70	21	3	0	100.0	99	88	8.5	0	0	0	1	25	72	2	0	0	100.0	n.d.	26
Neuquén	1	6	28	63	2	0	100.0	99	94	3.3	0	7	6	12	32	38	6	0	0	100.0	66	46
Negro	1	34	28	36	1	1	100.0	88	82	2.8	0	10	0	6	32	45	6	0	0.5	100.0	31	42
Coastal provinces																						
Río de la Plata	4	30	47	20	3	0	100.0	88	83	3.0	2	8	2	32	25	29	0	0.4	0.3	100.0	70	46
Mar del Plata	2	52	25	22	1	0	100.0	84	83	1.2	1	8	8	5	51	27	0	0	0.5	100.0	86	66

(Continues)

TABLE 1 (Continued)

River	Sample	Q	F	Lvm	Lsm	Lm^h		P/F	Vm/V	tHMC	ZTR	Ep	Grt	Amp	Cpx	Opx	Ol	Ap	&tHM		ACI	Cpx/Px
Bahía Blanca	5	28	36	35	1	0	100.0	89	89	3.1	0.5	5	3	10	45	34	2	0	0.2	100.0	74	56
Bahía San Blas	2	26	33	39	1	1	100.0	86	90	9.6	0	6	1	10	28	53	2	0.5	0.8	100.0	52	35
Pared del Golfo	7	22	37	40	1	1	100.0	87	90	7.0	0.1	5	0.8	8	35	50	0.1	0.1	0.3	100.0	62	41

Abbreviations: ACI, Amphibole Colour Index; Amp, amphibole; Ap, apatite; Ep, epidote; F, feldspar (P, plagioclase); Grt, garnet; L, aphanitic lithic fragments (Lvm, volcanic and low-rank metavolcanic; Lm^h, high-rank metamorphic); Lsm, sedimentary and low-rank metasedimentary; Ol, olivine; Px, pyroxene (Cpx, clinopyroxene; Opx, orthopyroxene); Q, quartz; tHMC, transparent heavy-mineral concentration; V, volcanic rock fragments (Vm, mafic and intermediate); ZTR, zircon + tourmaline + rutile.

and orthopyroxene. Apatite is significant in Río Mendoza. The moderately rich tHM suite of Río Tunuyán sand contains subequal amounts of amphibole, orthopyroxene and clinopyroxene. The rich tHM suites of Río Atuel sand is dominated by orthopyroxene and clinopyroxene with subordinate amphibole and minor olivine, epidote and garnet.

Detritus shed by the Sierra Pie de Palo is radically distinct from Andean detritus, being feldspatho-litho-quartzose with abundant high-rank metapelite, metapsammite and amphibolite rock fragments, and common muscovite and biotite (Figure 5f). The very rich tHM suite is dominated by mostly blue-green hornblende and garnet, with minor epidote and rare kyanite.

5.2 | Río Colorado and tributaries

Río Colorado carries to the Atlantic Ocean quartzo-feldspatho-lithic, plagioclase-dominated sand with mostly lathwork to microlitic volcanic lithics (Figure 6a). The moderately rich tHM suite mostly consists of clinopyroxene and orthopyroxene, with minor amphibole (green-brown hornblende and oxyhornblende), garnet and olivine. The upstream branches carry feldspatho-lithic (Río Barrancas) or quartzo-feldspatho-lithic (Río Grande; Figure 5b), plagioclase-dominated volcaniclastic sand with lathwork to microlitic, carbonate (mostly sparite) and locally siltstone and shale grains. The rich tHM suite, dominated by clinopyroxene prevailing over orthopyroxene, includes subordinate green-brown to brown hornblende and oxyhornblende, olivine and minor epidote and garnet (Figure 6d,e).

5.3 | Río Negro and tributaries

Río Negro transports to the Atlantic Ocean feldspatho-quartzo-lithic, plagioclase-dominated sand with mostly microlitic to lathwork volcanic lithics (Figure 6). The moderately rich tHM suite mostly consists of orthopyroxene and clinopyroxene, with epidote and minor olivine and blue-green to green-brown hornblende. Sand carried by the Limay, Neuquén, and Collon Cura rivers is feldspatho-lithic, with plagioclase and mostly lathwork and subordinate microlitic and felsitic volcanic lithics. Moderately rich to rich tHM suites consist of orthopyroxene prevailing over clinopyroxene, with minor hornblende, epidote, and olivine. Litho-feldspathic sand of Río Agrio is particularly rich in plagioclase and orthopyroxene (Figure 5c). Río Neuquén carries some garnet grains. Río Picun Leuvú (*picun*, north) carries feldspatho-quartzo-lithic sand including K-feldspar, volcanic but also carbonate, shale, slate and other

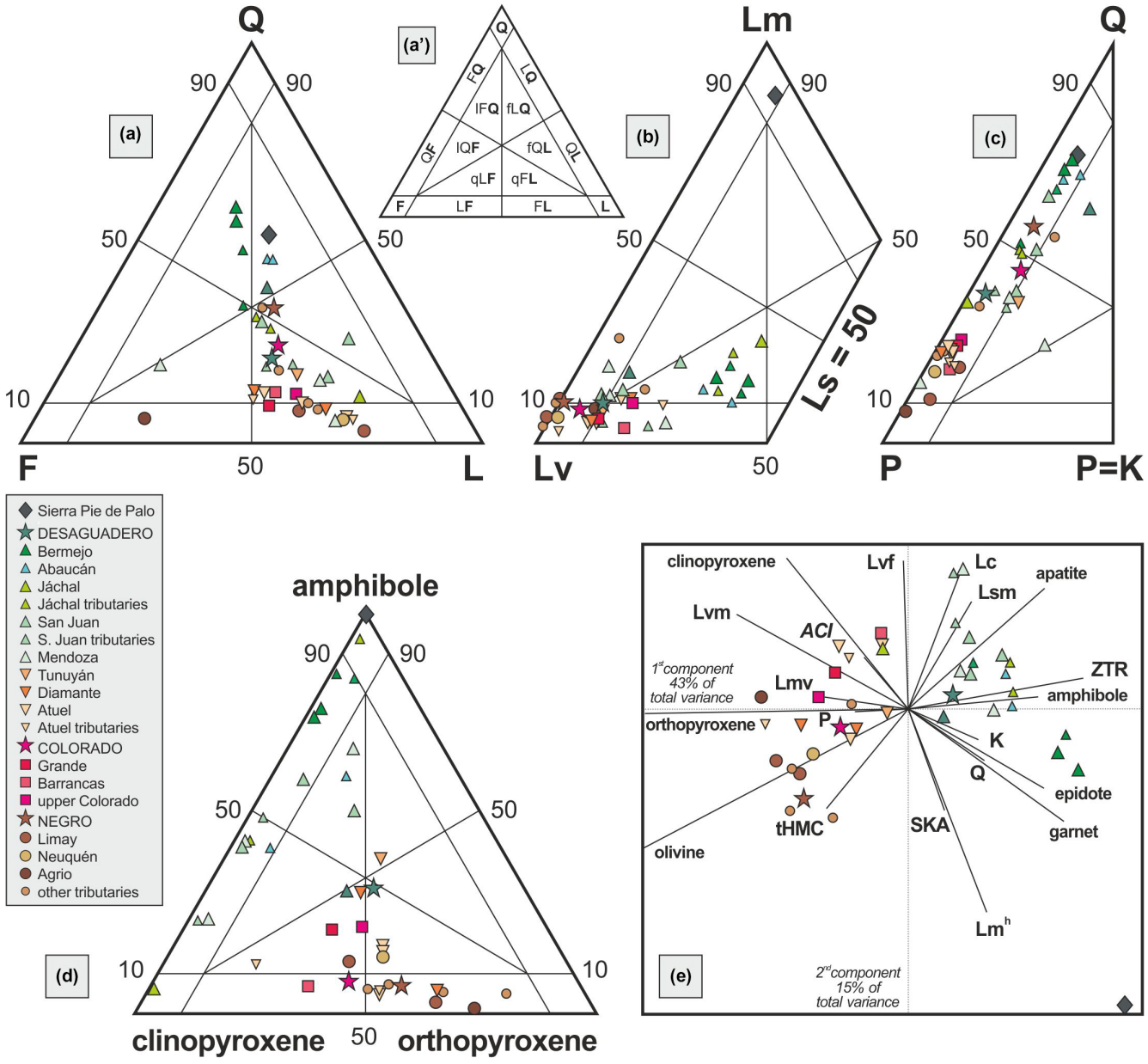

FIGURE 6 Framework-petrography and heavy-mineral modes. (a) River sands from the Andes are mostly quartzo-feldspatho-lithic (Colorado and Desaguadero), but range from feldspatho-lithic (Limay, Neuquén) to feldspatho-litho-quartzose (Abaucán) and litho-feldspatho-quartzose (Bermejo). (A′) Classification scheme (Garzanti, 2019). (b) Lithic fragments are mostly volcanic-derived, but sedimentary lithics become common in the north (Bermejo, Jáchal) and metamorphic lithics are shed by the Sierras Pampeanas (Pie de Palo). (c) Quartz decreases progressively southwards, from Río Bermejo to Río Limay, with slight increase of the P/F ratio. (d) Five end-member tHM suites are distinguished from north to south: (i) amphibole > clinopyroxene (Bermejo); (ii) amphibole ≈ clinopyroxene (Mendoza, San Juan); (iii) amphibole ≈ clinopyroxene ≈ orthopyroxene (Tunuyán); (iv) clinopyroxene ≥ orthopyroxene (Colorado) and (v) orthopyroxene ≥ clinopyroxene (Negro). The Sierras Pampeanas (Pie de Palo) shed amphibole and garnet. (e) The biplot (Gabriel, 1971; CoDaPack software by Comas-Cufí & Thió-Henestrosa, 2011) visualizes both differences among samples (points) and relationships among variables (rays). If the angle between rays is 0°, 90° or 180°, then the corresponding variables are correlated, uncorrelated or anticorrelated, respectively. Q = quartz; F = feldspar (P = plagioclase; K = K-feldspar); L = lithics (Lm = metamorphic; Lv = volcanic; Ls = sedimentary; Lvf = felsic volcanic; Lvm = mafic and intermediate volcanic; Lmv = low-rank metavolcanic; Lc = carbonate; Lsm = other sedimentary and low-rank metasedimentary; Lm^h = high-rank metamorphic); tHMC = transparent heavy-mineral concentration; ZTR = zircon + tourmaline + rutile; SKA = staurolite + andalusite + kyanite + sillimanite

sedimentary, very-low-rank metasedimentary and metavolcanic rock fragments, common olivine and minor zircon grains.

5.4 | Argentine coastal sand

Beaches and aeolian dunes south and north of the Río Negro mouth (Pared del Golfo and Bahía San Blas coastal provinces defined in Garzanti et al., 2021, from which the following information is taken) consist of quartzo-litho-feldspathic to quartzo-feldspatho-lithic, plagioclase-dominated volcaniclastic sand with orthopyroxene, clinopyroxene and minor amphibole and epidote. Beaches and aeolian dunes north of the Río Colorado mouth (Bahía Blanca coastal province) consist of quartzo-feldspatho-lithic, plagioclase-dominated volcaniclastic sand, with clinopyroxene, orthopyroxene and minor amphibole, epidote and garnet. North of the Tandil High, sand is litho-feldspatho-quartzose, reflecting additional sediment supply from sea cliffs.

The hook-shaped Samborombón Bay to the north has no sand. Only mud is deposited in this flat wetland underlain by shell ridges, either from very-low-gradient distributary channels draining the salt marshes or from the Paranà River in flood. The tHM suites of Río Salado mud near the mouth and of Río de la Plata beach sand as far as Buenos Aires are much richer in amphibole than beach sand to the south.

6 | PROVENANCE OF RIVER SAND

The Andes largely consist of geological units extending roughly parallel to strike for thousands of kilometres (e.g. mesosilicic volcanic rocks of the Cordillera Principal). Orogenic detritus generated in the study area and fed into the retroarc basin consequently displays broadly similar compositional signatures, characterized by intermediate to mafic volcanic rock fragments, plagioclase and generally rich tHM suites dominated by clinopyroxene (green augite), orthopyroxene (hypersthene) and brown magmatic hornblende and oxyhornblende in different proportions, with minor olivine, apatite or zircon locally (Table 1). Despite several similarities, however, sediments carried by major river systems in this area can be confidently discriminated, and compositional trends from north to south are manifest. They reflect both the different lithological units exposed along the retroarc-side of the Andes or within the broken retroarc basin (Figure 4) and the different characteristics and crystallization conditions (mafic vs. felsic, lower vs. higher temperature or pressure and alkali or water content; Gill, 1981, ch. 6) of arc magmas through time and space (Deruelle, 1982; Kay et al., 2005).

These geological and mineralogical factors are all decisively influenced by subduction geometry. A gap in magmatic activity and greater structural elevation with wider exposure of deeper-seated tectono-stratigraphic basement levels both in the cordillera and in the adjacent retroarc basin characterize the Pampean flat-slab segment, in contrast with the extensive Quaternary Payenia basaltic lava field corresponding to the less-shallow-subduction segment in the south (Figure 7a). Because of different source-rock lithologies, river-sand composition ranges from feldspatho-litho-quartzose (Abaucán) or litho-feldspatho-quartzose (Bermejo) in the north (28°–30°S), to mostly quartzo-feldspatho-lithic in the centre (30°–34°S; Jáchal, San Juan, Mendoza, and Tunuyán) and feldspatho-lithic in the south (34°–41°S; Atuel, Neuquén and Limay) (Figure 7b). The tHM suite composition also changes, being characterized by amphibole ≫ pyroxene in the north (Bermejo), by amphibole ≈ clinopyroxene ≫ orthopyroxene in the centre-north (San Juan and Mendoza), by amphibole ≈ clinopyroxene ≈ orthopyroxene in the centre (Tunuyán), by clinopyroxene ≥ orthopyroxene ≫ amphibole in the centre-south (Río Colorado catchment) and by orthopyroxene ≥ clinopyroxene ≫ amphibole in the south (Río Negro catchment) (Figure 7b). The abundance of quartz, K-feldspar, sedimentary to low-rank metasedimentary rock fragments, and amphibole, thus, reaches maximum in correspondence with the Pampean flat-slab segment where volcanism is inactive, whereas volcanic detritus from the Cordillera Principal and Payenia lava flows becomes progressively overwhelming southwards (Figure 7).

Five end-member sources of detritus can be identified, based mainly on rock fragments and heavy minerals: (a) lathwork volcanic rock fragments, clinopyroxene and olivine distinctive of mafic lavas (e.g. Payenia basalts; Søager et al., 2013); (b) mainly microlitic volcanic rock fragments, plagioclase, clinopyroxene, and either brown amphibole or orthopyroxene distinctive of andesites and dacites of the Cordillera Principal (Deruelle, 1982; Kay et al., 2005); (c) felsitic volcanic to low-rank metavolcanic rock fragments distinctive of rhyolites of the Permian–Triassic Choiyoi Group (Kleiman & Japas, 2009); (d) sedimentary/metasedimentary rock fragments, quartz, K-feldspar and ZTR minerals distinctive of sedimentary to metasedimentary rocks exposed in the Precordillera (Allmendinger & Judge, 2014); (e) high-rank metamorphic rock fragments, quartz, feldspars, micas, blue-green amphibole and garnet distinctive of basement blocks uplifted in the Sierras Pampeanas (Rapela et al., 2010).

The contribution of these diverse end-member sources to each river system and the varying proportions of detritus

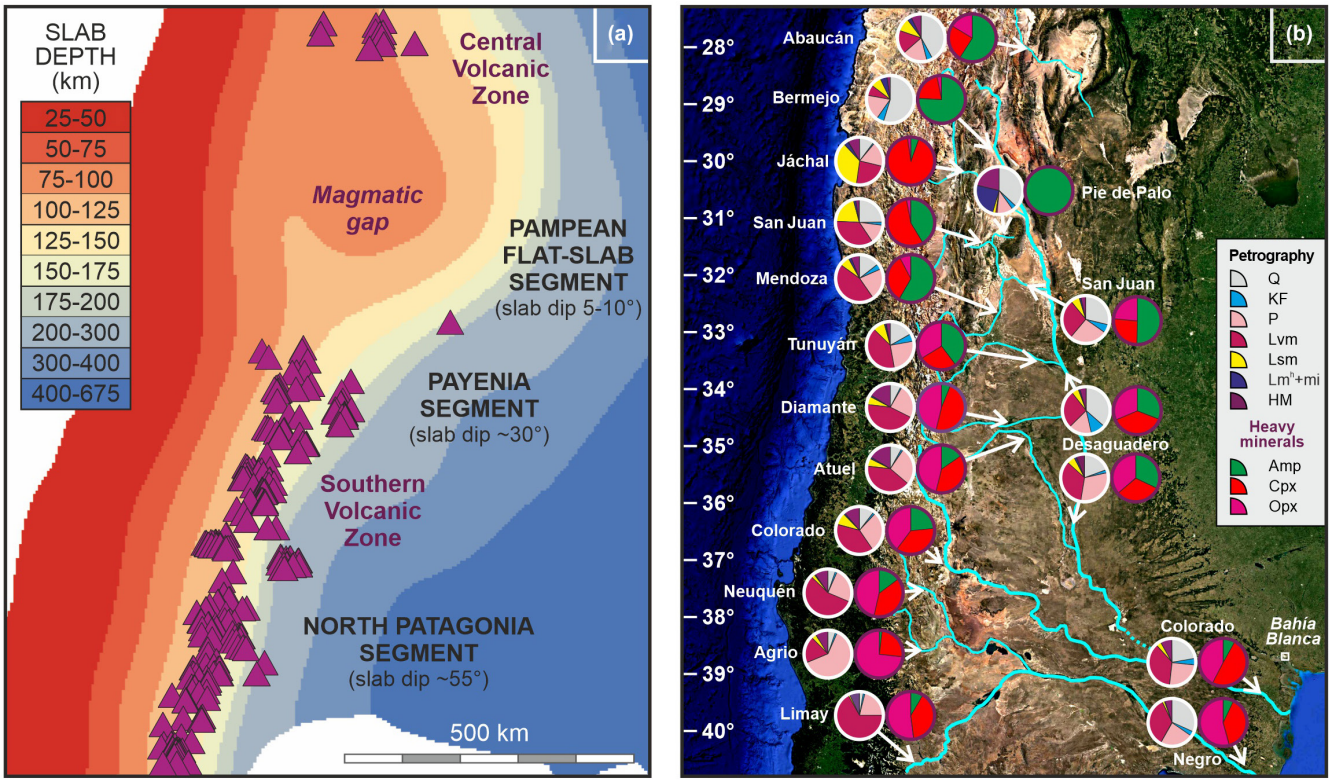

FIGURE 7 Relationships among subduction geometry, magmatic activity and sediment composition. (a) The Pampean flat-slab segment corresponds to a magmatic gap, highest structural elevation and exposure of deeper-seated tectono-stratigraphic basement levels of the Andean orogen (slab depth after Capaldi et al., 2021). (b) Abundance of quartz (Q), K-feldspar (KF), sedimentary to low-rank metasedimentary rock fragments (Lsm) and amphibole (Amp) all reach maximum in coincidence with the magmatic gap and decrease southwards, where volcanic to low-rank metavolcanic rock fragments (Lvm), plagioclase (P) and pyroxene derived from the Southern Volcanic Zone progressively increase. The ratio between clinopyroxene (Cpx) and orthopyroxene (Opx) increases with the mafic character of the eroded volcanic products (e.g. Payenia basalts). Lm^h + mi = high-rank metamorphic + mica

derived from volcanic, sedimentary and basement rocks in different tributaries and along the mainstem were tentatively assessed with forward mixing calculations (for a detailed illustration of methods and rationale see Garzanti et al., 2012; Resentini et al., 2017; further information is contained in Appendix A). Estimates derived from such calculations are provided in the subsections below.

6.1 | Upper Desaguadero (Bermejo) catchment

The geological units drained by the Abaucán, Bermejo, Jáchal, San Juan and Mendoza rivers in the northern part of the study area include the igneous rocks of the Cordillera Frontal, the sedimentary to low-grade metasedimentary rocks of the Precordillera and the amphibolite-facies basement rocks of the Sierras Pampeanas. The Cordillera Principal here drains mostly towards Chile and a limited amount of detritus from Mesozoic and Cenozoic arc rocks is fed into the retroarc basin mixed with detritus from the bimodal (basal mafic and upper felsic) rocks of the Permian–Triassic Choiyoi igneous complex. Palaeozoic strata of the Precordillera supply sedimentary and metasedimentary rock fragments and polycyclic detritus originally derived from arc and basement rocks. The intermontane valleys across the Precordillera are floored by Neogene retroarc-basin deposits consisting of Andean arc material and these sediments are extensively recycled in modern rivers owing to their erodibility and high sand-generation potential, as documented by detrital-zircon geochronology (Capaldi et al., 2017).

Composition of Abaucán and Bermejo river sand in the north is distinct from that of San Juan and Mendoza river sand in the south (Figure 7b). Quartz is three times more abundant in the north, whereas volcanic lithics and clinopyroxene are three times more abundant in the south. In the north, high-rank metamorphic lithics, blue-green amphibole, garnet and rare kyanite and sillimanite document minor contributions from amphibolite-facies basement rocks of the Sierras Pampeanas. Upper Río Bermejo sand

consists of common quartz, ZTR minerals, some feldspars, carbonate, sandstone and pelite rock fragments derived from Lower Palaeozoic strata of the Precordillera (≥50%), with subordinate volcanic detritus (30%–40%) and minor contributions from metamorphic rocks of the Sierras Pampeanas (ca. 10%). Detritus from Silurian–Devonian shales, slates and phyllites of the Precordillera reaches maximum (ca. 40%) in Río Jáchal sand, where dominant clinopyroxene is plausibly recycled from Neogene retroarc-basin volcaniclastic deposits (Capaldi et al., 2017; Gonzalez et al., 2020).

The San Juan and Mendoza rivers, which mainly drain the Cordillera Frontal and the Precordillera, carry sand with similar detrital signatures. Carbonate and pelitic rock fragments are common in the headwaters, indicating contributions from Jurassic-Cretaceous strata exposed along the eastern rim of the Cordillera Principal (Aconcagua fold-thrust belt; Mpodozis & Ramos, 1989). The amount of felsitic volcanic to very-low-rank metavolcanic rock fragments, largely derived from the Permian-Triassic Choiyoi Group, remains relatively constant downstream in both rivers (Figure 6). Sedimentary detritus, including slate and metasiltstone rock fragments shed from Silurian–Devonian strata of the Precordillera, increases downstream of Río San Juan. Río Mendoza sand at the mountain front is uniquely characterized by K-feldspar, biotite and mostly felsic to intermediate but also mafic igneous/metaigneous rock fragments. This peculiar signature indicates limited supply from Palaeozoic strata of the Precordillera and may be accounted for by sequestering of a large part of the bedload fraction in the Potrerillos Reservoir upstream (De Doncker et al., 2020) and consequently largely local detrital supply from Permian–Triassic granite to monzonite intrusions (Cingolani et al., 2012). This is supported by somewhat lower ACI in this sample and U-Pb zircon-age spectrum characterized by a unimodal Permian–Triassic peak (figure 5 in Capaldi et al., 2017). The effect of sediment trapping in artificial reservoirs is also manifest for the Rio Jáchal sample collected downstream of the Cuesta del Viento Dam, which displays a peculiar composition sharply distinct from sand in its upstream branch Río Iglesia and including abundant shale/slate rock fragments derived from locally exposed Palaeozoic strata of the Precordillera (Figure 4).

Along the Bermejo–Desaguadero trunk river, the volcanic component of detritus is calculated to decrease from ca. 40% close to the mountain front to ca. 20% upstream of the Médanos Grandes and then to increase again to ca. 35% downstream of the Tunuyán confluence. Conversely, detritus from Sierras Pampeanas basement rocks first increases from ca. 10% to 30% and then decreases to <20%. Sedimentary detritus invariably accounts for half of the sand.

6.2 | Lower Desaguadero catchment

The geological units drained by the Tunuyán, Diamante and Atuel rivers include the Cenozoic volcanic rocks of the Cordillera Principal and the Quaternary Southern Volcanic Zone, the Jurassic–Cretaceous retroarc strata of the Malargüe fold-thrust belt containing detritus from Andean arc rocks presently exposed in Chile, and Devonian–Carboniferous strata with the overlying Permian-Triassic Choiyoi volcanics uplifted in the San Rafael Block (Kleiman & Japas, 2009). The Diamante and Atuel rivers cut across the northern tip of Quaternary Payenia basaltic fields exposed across the San Rafael uplift.

Tunuyán river sand has composition similar to San Juan and Mendoza sands, but with a much higher Vm/V ratio and much lower Cpx/Px ratio, suggesting supply from the northern edge of the Southern Volcanic Zone along with recycling of retroarc-basin strata (Porras et al., 2016).

In Diamante and Atuel sands, dominant andesitic to basaltic detritus derived from both the Cordillera Principal and the Payenia volcanic province is associated with only minor sedimentary to low-rank metasedimentary detritus derived from the Malargüe fold-thrust belt or San Rafael Block. Quartz, K-feldspar and the ZTR index are lowest relative to all studied catchments, whereas the tHMC index is highest, indicating minimum recycling of siliciclastic rocks. Prevalence of andesitic to dacitic detritus from the Cordillera Principal is indicated by Cpx/Px <50%, whereas minor olivine is plausibly shed from Payenia basalts.

Along the Desaguadero trunk river, volcanic detritus is estimated to reach ca. 70% upstream of the Atuel confluence, where sedimentary detritus and contribution from basement rocks of the Sierras Pampeanas are reduced to 20% and ≤10%, respectively. Locally abundant celestite grains were considered as intrabasinal in origin and reworked from evaporite crusts formed in the floodplain or even within the river channel during dry seasons. Erosion of barite and celestite ores sparsely hosted in mid-Jurassic to Lower Cretaceous evaporites (Ramos & de Brodtkorb, 1990) is considered less likely because of rare exposures, limited clast durability and only local accumulations.

6.3 | Colorado and Negro catchments

Cenozoic andesites of the Cordillera Principal and basalts of the Payenia province represent the dominant sources of detritus for the Grande and Barrancas headwater branches of Río Colorado. Composition is, thus, similar to Atuel sand, but with greater contribution from Payenia basalts as reflected by Cpx/Px >50%. Río Colorado sand near the coast is roughly estimated to be derived approximately

two thirds from volcanic rocks and one third from sedimentary rocks.

Detritus from the Payenia volcanic province is negligible in the Río Negro catchment to the south, where dominant provenance from andesites and dacites of the Cordillera Principal is reflected by Cpx/Px <50% in most tributary sands. Río Picun Leuvú extensively drains Jurassic–Cretaceous sedimentary rocks of the Neuquén Basin, as reflected by markedly higher quartz, K-feldspar, carbonate and shale rock fragments and by an only moderately poor tHM suite with significant ZTR minerals. Volcanic detritus includes olivine derived from olivine basalts emplaced in the retroarc region during different Oligo-Miocene to Pliocene stages (Kay & Copeland, 2006; Leanza et al., 2001). Similar feldspar ≤ quartz ≤ lithics composition characterizes Río Negro sand near the coast, indicating significant contribution (≤40% of total sand) from sedimentary rocks of the Neuquén Basin.

7 | THE KNIGHT'S MOVE: TRANSCONTINENTAL TRANSPORT FOLLOWED BY LITTORAL DRIFT

The petrographic and mineralogical signatures of sediment generated in the Andes and conveyed towards the Atlantic Ocean by the Desaguadero, Colorado and Negro rivers allowed us to trace a huge Quaternary sediment dispersal system that bypasses the retroarc basin and continues at right angles for several hundreds of kilometres along the Argentine passive-margin shores (Garzanti et al., 2021).

7.1 | Tectonic control on fluvial transport across the broken retroarc basin

In central Argentina, strong tectonic control on sediment transport is exerted by basement uplifts within the broken retroarc basin (Figure 2), including the Sierras Pampeanas in the north, the San Rafael block in the west, the Pampa Central block in the east (La Pampa High, including the Chadileuvú block; Nivière et al., 2013), and the North Patagonian Massif in the south (Alicia Folguera et al., 2015). The sediment route towards the Atlantic Ocean is, thus, confined to a narrow latitudinal transfer zone (i.e. Colorado and Negro river valleys) delimited by these broad uplifted retroarc regions (Figure 8).

The structure and relief of the retroarc basement is related to the subduction geometry of the Nazca Plate. Very shallow slab dips (ca. 5°–10°) in the Pampean segment, likely related to subduction of the Juan Fernández seamount chain (Stern, 2020; Yáñez et al., 2001), are associated with greatest amount of Andean shortening and most pronounced basement uplifts within both the Andes (Aconcagua fold-thrust belt, Cordillera Frontal and Precordillera) and the adjacent basin (Sierras Pampeanas), reaching topographic elevations of nearly 7,000 m in the orogen and above 6,000 m in the broken retroarc region. As subduction angle increases southwards, from ca. 30° in the Payenia segment to ca. 55° in northern Patagonia (Figure 7a), the retroarc basin is partitioned by broader, low-relief structures (San Rafael-Pampa Central Block and North Patagonian Massif). The age of the Andean arc also changes along strike, being predominantly Miocene in the Pampean segment and Cretaceous in northern Patagonia.

In the actively uplifting segment of the Andes where elevation approaches 7,000 m a.s.l. (Lossada et al., 2018), rugged relief and slope instability, coupled with intense seismicity and extreme climatic events, trigger large landslides and debris flows as major agents of sediment generation (e.g. Hermanns et al., 2015; Moreiras et al., 2021; Vergara et al., 2020). However, because of dry climate, erosion rates are estimated to reach only moderate annual values up to ca. 0.3 mm near 34°S on both sides of the range, based on gauged suspended sediment and cosmogenic nuclides (Carretier et al., 2018; Val et al., 2018). Higher annual values ≥1 mm were estimated for the Mendoza catchment based on siltation rate of the Potrerillos reservoir (De Donker et al., 2020).

The Pampean flat-slab segment from 27° to 33°S, corresponding to the magmatic gap between the Central and Southern Volcanic Zones, coincides with the highest topographic and structural elevations in the Cordillera Principal, Cordillera Frontal, Precordillera, as in the uplifted basement blocks of the broken retroarc basin (Figure 3a; Ramos et al., 2002; Stern, 2004). Compressional tectonics and dynamic uplift of the retroarc region (Dávila & Lithgow-Bertelloni, 2015; Siame et al., 2005) exerted a direct control on the evolution of the drainage network. The course of Río Bermejo is funnelled along the trace of the NW/SE-trending fault bounding the Sierra Valle Fértil uplift (Figure 8). Downstream, the Río Desaguadero mainstem descends the retroarc basin axially along a structurally controlled slope away from the culmination of the Sierras Pampeanas basement uplifts.

The style of retroarc-basin deformation changes farther south, where uplift of the Pampa Central Block may represent a flexural bulge induced by the eastward propagation of Andean deformation since the late Miocene (La Pampa High of Nivière et al., 2013). The southward-progressing uplift of the bulge determined the stepwise southward shift of the Río Desaguadero course, which left a mark in the six main ≥100 km-long, 1–2 km-wide and ≤100 m-deep '*valles trasversales*', paleochannels formerly directed towards the swampy Pampa Deprimida backbulge (Figure 8; Pampa

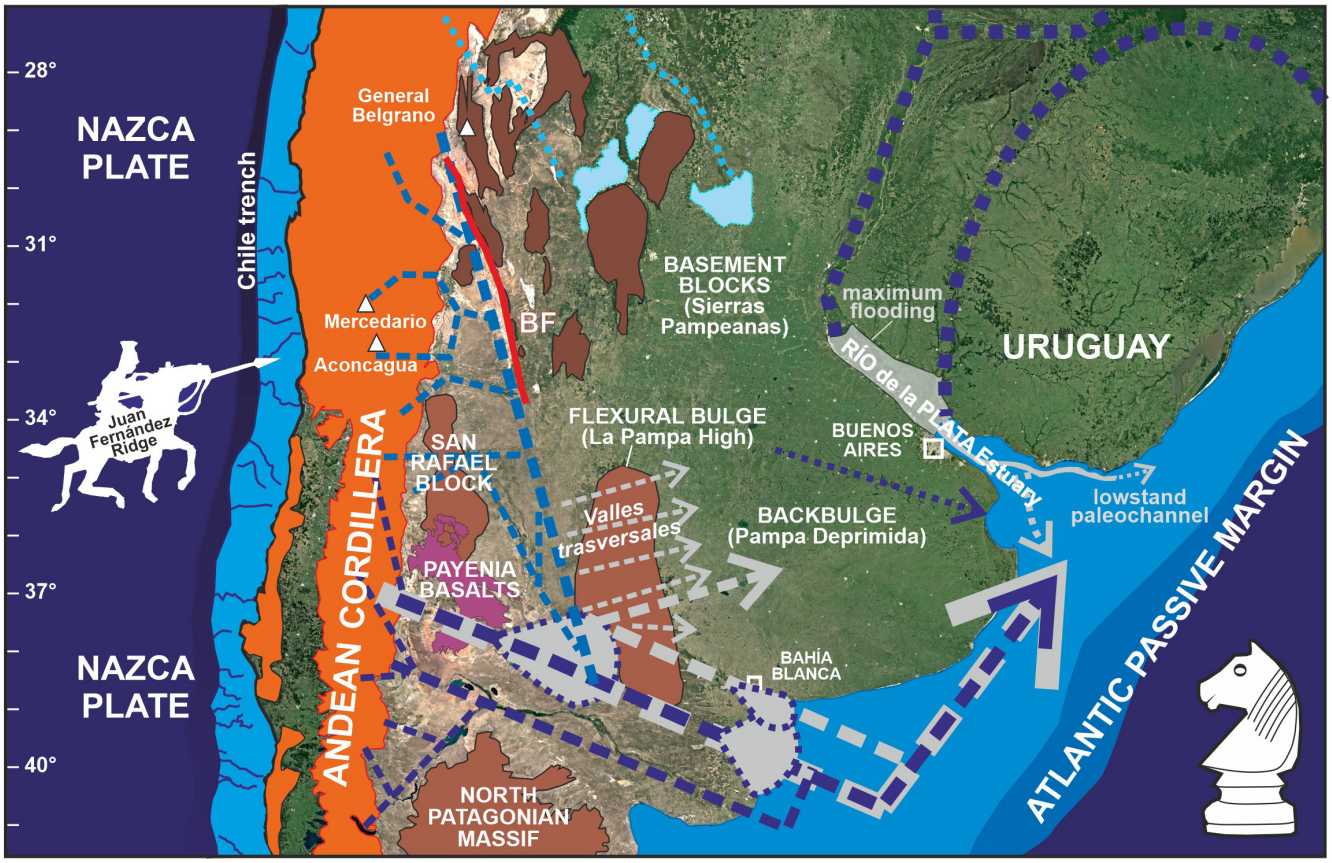

FIGURE 8 Tectonically controlled trajectories of transcontinental sediment dispersal in time (present: blue dashed arrows; past: grey dashed arrows and shaded areas). In the north, Río Desaguadero follows the Bermejo fault (BF; red line) and descends between the uplifted blocks of the broken retroarc basin along a slope that parallels the southward-increasing angle of the subducting Nazca Plate. In the south, Río Negro skirts around the Northern Patagonian Massif and flows side by side with Río Colorado. All volcaniclastic sediment generated from a 1,600-km-long tract of the Andes, thus, reaches the Atlantic passive margin almost in the same point. During the Plio-Pleistocene, southern rivers could initially flow directly eastwards but were displaced stepwise by the southward progressing flexural wave, leaving their mark in the *Valles trasversales*. Río Desaguadero and Río Colorado eventually joined and the sediment mass transported during deglaciation or humid stages fed alluvial fans inland and large deltaic lobes at sea (Spalletti & Isla, 2003; Vogt et al., 2010). Transport direction here changes from eastwards to northwards (the knight's move) and sand entrained by swell-induced longshore currents reaches as far north as Río de la Plata. Glacio-eustatic changes forced the Río de la Plata coastline to shift landward and seaward by up to ca. 700 km (Violante & Parker, 2004). In the present dry climate, Río Abaucán and Río Desaguadero have become endorheic (lighter blue colours)

Sur in Iriondo, 1994). Abandonment of these channels indicates that flexural uplift outpaced stream power during dry climatic stages.

Progressive southward migration led Río Desaguadero to flow along a broad open valley meeting the Atlantic coast at Bahía Blanca (Perillo et al., 2001) and, finally, to become confined in the narrow strip between the San Rafael Block and the Chadileuvú block, join Río Colorado and feed a large single delta south of Bahía Blanca (Melo et al., 2003; Spalletti & Isla, 2003). Equally dictated by tectonic regime is the course of the Colorado and Negro rivers, funnelled between the San Rafael block to the north and the North Patagonian Massif to the south, where they run subparallel to each other, locally only ca. 40 km apart (Figure 8).

7.2 | Littoral transport of volcaniclastic sand along the Argentine passive margin

Sediment generated from the 1,600-km-long eastern flank of the Central and Southern Andes between ca. 27° and 41°S is transferred eastwards via the Desaguadero, Colorado and Negro rivers, reaching the Atlantic Ocean at two entry points lying only 190 km apart (39°40′S and ca. 41°S). Beyond the Negro and Colorado river mouths, sand transport changes to mostly northwards and parallels the Atlantic shoreline for nearly 1,000 km (Garzanti et al., 2021). This composite cell of littoral sand drift was generated by swells and winter storms prevalently from the south and extends as far as the southern mouth of Río de la Plata estuary. All along this tract of the Argentine coast, sand is, thus, dominantly (ca. 70%)

volcaniclastic, similar to detritus shed by magmatic arcs and quite unusual for a rifted margin (Garzanti et al., 2001, 2014). Such a discrepancy between the geodynamic setting of the source and the depositional sink has been long recognized (Blasi & Manassero, 1990; Potter, 1984, 1994) and a similar mismatch caused by transcontinental sediment transfer over thousands of kilometres occurs in other orogenic regions worldwide (e.g. Vezzoli et al., 2016).

Besides the relative proportions of felsitic, microlitic and lathwork volcanic rock fragments, preferentially derived from rhyodacite, andesite and basalt, respectively (Affolter & Ingersoll, 2019; Dickinson, 1970; Le Pera & Morrone, 2020; Marsaglia & Ingersoll, 1992), the Cpx/Px ratio and the percentage and colour (ACI) of detrital amphibole (Andò et al., 2014) provide the most diagnostic tracers for longshore sediment dispersal. In the ca. 1,200-km-long coastal stretch from San Antonio to the Río de la Plata (Figure 1), beach and dune sand remains mainly quartzo-feldspatho-lithic to quartzo-litho-feldspathic. However, abundant orthopyroxene and lower ACI indices characterize the southern tract, indicating major influence of the Río Negro, whereas clinopyroxene prevails over orthopyroxene and ACI indices are notably higher north of the Río Colorado mouth, revealing dominant supply from the Río Colorado (Garzanti et al., 2021).

7.3 | Processes controlling generation and long-distance transfer of volcaniclastic sediment

Sedimentation in central Argentina is controlled by three main factors: (a) intense subduction-related tectonic and magmatic activity in the Andean cordillera, leading to the development of high relief, slope instability, rapid erosion, and efficient sediment production via landslides and debris flows (Moreiras & Sepúlveda, 2015); (b) limited or even negative storage capacity in the retroarc basin, caused by inversion tectonics and articulated basement uplifts associated with changing geometries of the subducting Nazca Plate (Capaldi et al., 2020) and (c) arid climate in the retroarc region, leading to inefficient fluvial transport, sediment dumping, wind deflation and sand accumulation in dune fields (Zárate & Tripaldi, 2012).

High sediment supply in the highlands and limited sediment sequestration in the lowlands would lead to efficient transfer of huge detrital volumes to the Atlantic Ocean if not impeded by scarce rainfall and, therefore, reduced river discharge and sediment-transport capacity, which characterize the present and past stages with dry climate and limited glacial cover. Transport efficiency, however, was greatly augmented during deglaciation stages of the Pleistocene to early Holocene, when large amounts of water were released by melting of the Cordilleran ice sheet, or during pluvial events characterized by higher precipitation over sufficiently long periods (Iriondo & Garcia, 1993; Martinez & Kutschker, 2011). The swollen sediment-laden waters of the Desaguadero and Colorado rivers then rushed from the highest-relief tract of the Andes, fostering alluvial fans and floodplains inland (Vogt et al., 2010) and flowing towards the Atlantic Ocean in much larger valleys than today (Zárate & Blasi, 1993). Sand and gravel supply to the coast was high enough not only to promote rapid progradation of deltaic lobes and form a ca. 200-km-wide deltaic complex (Spalletti & Isla, 2003) but also to feed the cell of littoral sediment transport extending for hundreds of kilometres along the coast of the Buenos Aires Province (Figure 8). Water discharge and consequently stream power, flow competence and sediment fluxes have been strongly reduced since the last deglaciation stage (Zárate & Blasi, 1993). The present dry climate impacted the most the Río Desaguadero, which drains the tract of the Cordillera where elevation and relief are highest, until it became virtually disconnected from the Colorado mainstem (Nivière et al., 2013). Because of drastically decreased sediment supply, the Colorado delta was extensively reworked by tides and waves during the late Holocene sea-level rise (Melo et al., 2003).

8 | TECTONICS AND SEDIMENTATION IN RETROARC BASINS

Different types of orogenic belts are associated with three main types of sedimentary basins floored by continental crust (as defined in Garzanti, 2020): (a) foreland basins, formed on the lower plate undergoing E/NE-dipping continental subduction (e.g. Indo-Gangetic plain; Burbank et al., 1996); (b) foredeeps, formed on the lower plate undergoing W-dipping continental subduction (e.g. Apenninic foredeep; Carminati & Doglioni, 2012) and (c) retroarc basins, formed on the upper plate of an E-dipping oceanic subduction (e.g. Andean retroarc basin; Jordan, 1995).

These three basin types coincide, respectively, with the collisional, retreating-collisional and retroarc foreland-basin systems illustrated in DeCelles (2012). The fundamental difference with the widely adopted depositional model of DeCelles and Giles (1996) – underscored by the choice of a partly different nomenclature – lies in the observation that depozones have different character and architecture in these three types of basins formed by profoundly different subsidence mechanisms. A flexural component proportional to the size (load) of the orogen is present in all three cases, although dominant only for retroarc basins (Naylor & Sinclair, 2008; Sinclair & Naylor, 2011). Larger orogens, such as the Alps, the Himalaya or the Andes, exert

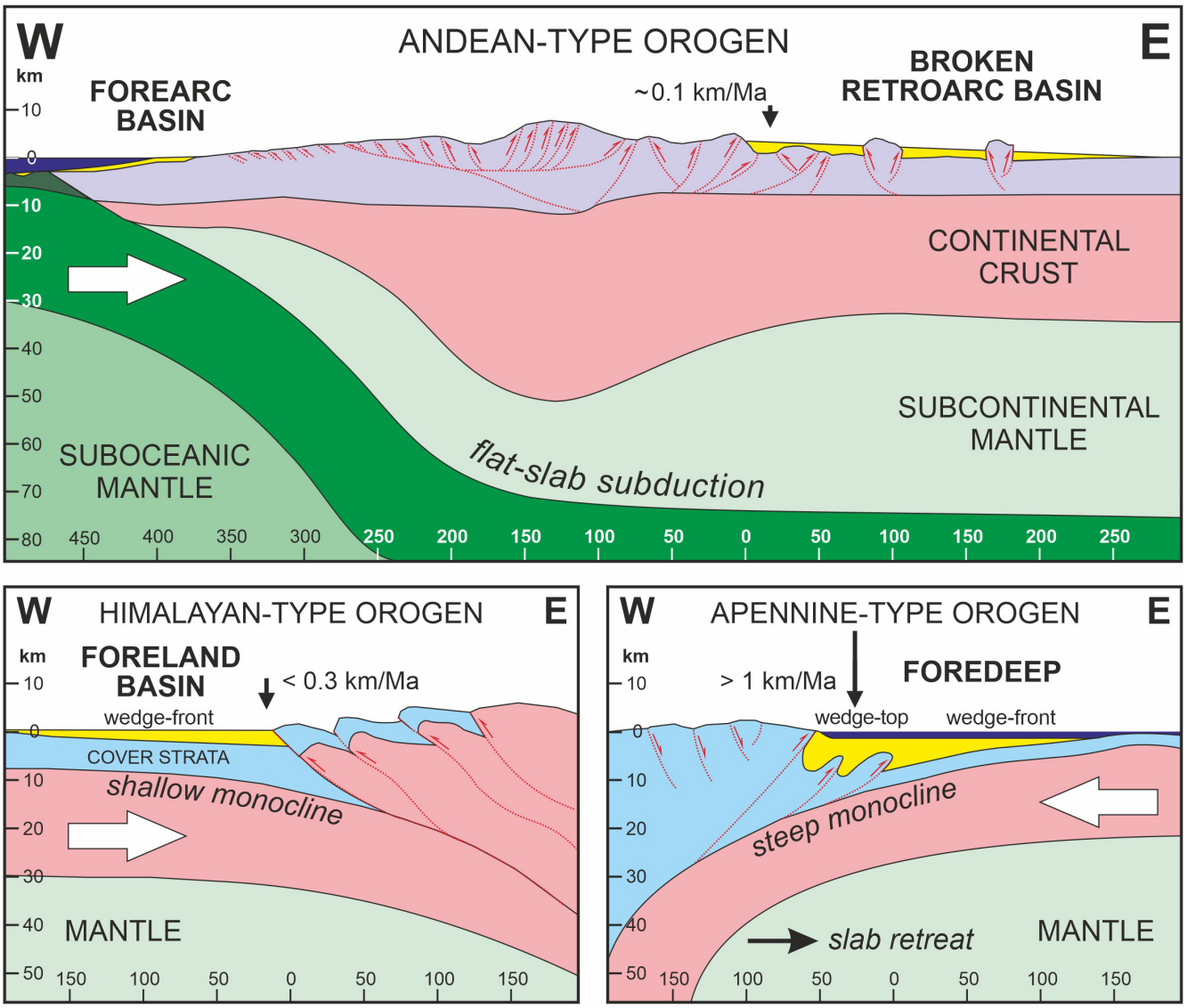

FIGURE 9 Three different orogen types associated with different types of sedimentary basins (subsidence rates after Doglioni & Panza, 2015). Sediment storage capacity is maximum in foredeeps, where rapid subsidence of both wedge-front and wedge-top depozones is induced by slab retreat, and minimum to even negative in broken retroarc basins, where flat-slab subduction leads to greater plate coupling, basin inversion and strong uplift of basement blocks

a stronger flexural effect, but they have less-subsident, typically overfilled associated basins relative to much smaller thrust belts such as the Carpathians or the Apennines, associated with much more rapidly subsiding, truly deep foredeeps (Doglioni, 1994). The Apennine belt itself has been so strongly subsident through time that remained covered by pelagic and turbiditic sediments for most of its history (Cibin et al., 2001). Strongly underfilled (deep) foredeep and wedge-top depozones hosting deep-water sediments exist only beside and on top of Apennine-type orogenic belts, where piggy-back basins were in fact originally defined (Ori & Friend, 1994). Foredeeps (i.e. deep-water basins hosting deep-water sediments) are not formed in the flexural moat of all types of orogens. To this misleading idea have contributed earlier studies of the Alpine foreland basin ('underfilled trinity model' of Allen et al., 2001; Sinclair, 1997), where turbidites were indeed deposited but only at an early stage when Europe ceased to be the lower plate of the Alpine subduction to become the upper plate of the Apenninic subduction and was, thus, affected by strong tectonic extension/transtension (Dèzes et al., 2004; Doglioni et al., 1999; Hu et al., in review). Orogenic sediments issued from the Alps, the Himalayas, or the Andes typically display marginal marine to continental 'molasse' facies.

The different geodynamic setting in which these three types of basins are formed implies a different system of applied forces, as reflected in radically different subsidence magnitude (Figure 9). Total long-term subsidence is an

order-of-magnitude higher for foredeeps associated with much smaller singly-vergent thrust-belts (>1 km/Ma) than for foreland basins (<0.3 km/Ma) and retroarc basins (even ≤0.1 km/Ma) associated with much larger doubly-vergent orogens (Doglioni & Panza, 2015). Large tracts of retroarc basins are actually uplifting rather than subsiding. Basement blocks reaching elevations of hundreds to several thousands of metres do not characterize foreland basins (with possible exceptions such as the Kirana Hills and Shillong Plateau at the opposite edges of the Indo-Gangetic Plain) and are certainly at odds with the rapid steady subsidence characterizing foredeeps. Loads and flexure, therefore, are demonstrably less important subsidence mechanisms than subduction-related dynamic processes, such as slab retreat in the case of foredeeps (Doglioni et al., 2007) or far-field effects associated with the geometry of the subducting slab in the case of retroarc basins (Dávila & Lithgow-Bertelloni, 2015).

As a consequence, sediment budgets and the ratio between what can and what cannot be stored within the basin and is, therefore, exported elsewhere are also notably different in these three cases. The entire, generally very small amount of detritus shed by Apennine-type thrust belts can be easily accommodated in the rapidly subsiding foredeep, which remains underfilled unless it is fed with sediment derived from external sources (e.g. the Alps in the case of the Apenninic foredeep; Garzanti & Malusà, 2008; Garzanti et al., 2011). Conversely, most of the huge detrital mass shed from Himalayan-type collision orogens or Andean-type cordilleras cannot be stored in the relatively small adjacent foreland or retroarc basin and it is, thus, exported away towards other depositional sinks, including passive margins and remnant-ocean basins (Figuereido et al., 2009; Graham et al., 1975; Limonta et al., 2015). Long periods of reduced or even inverted subsidence are documented in foreland and retroarc basins by the presence of major unconformities associated with stratigraphic gaps of up to 20 Ma (DeCelles & Horton, 2003; DeCelles et al., 2004; Horton et al., 2016), in contrast with prolonged accelerated subsidence characterizing both wedge-top and wedge-front depozones of foredeeps (Amadori et al., 2019; Ricci Lucchi, 1986).

Rough calculations indicate that only a minority of orogenic sediment produced by erosion of the Himalaya through time could be eventually accommodated in the adjacent foreland basin, estimated percentages ranging from 10% (Lupker et al., 2011; Sinha & Friend, 1994) or 20% (France-Lanord et al., 2016) to ≤30% (Clift et al., 2001; Einsele et al., 1996). Sediment budgets gave similar results for the foreland basin facing the western and eastern European Alps since the Oligocene (15%–20% retained and 80%–85% exported to the Rhône Fan, Apenninic foredeep and other sedimentary basins including the North Sea and Black Sea; Hinderer, 2012; Kuhlemann et al., 2002).

Along the Andes, much of the sediment generated from the cordillera cannot be stored permanently in the retroarc basin but it is exported to the Atlantic Ocean via the Orinoco River in the north (Gallay et al., 2019), via the Amazon River in the centre-north (one-third of sediment retained and two-thirds exported in the Madeira catchment; Vauchel et al., 2017), via the Andean sub-tributaries of the Paranà River in the centre-south (e.g. Pilcomayo and Bermejo rivers; Amsler et al., 2007), and *via* the studied Desaguadero-Colorado and Negro river systems in the south. The transfer of large masses of detritus from the Andean cordillera to the Atlantic Ocean is a consequence of the limited long-term storage capacity of the retroarc basin, where periods of rapid subsidence can be followed by tectonic inversion, uplift and erosion.

During stages of cratonward propagation of orogenic deformation, retroarc-basin sediments previously accumulated in flexural moats near the mountain front are accreted to the fold-thrust belt and recycled, whereas those deposited along the far side of the basin can be involved in flexural uplift and, thus, also eroded away. Tectonic inversion and recycling may be induced by changing subduction geometry, when reduction of the subduction angle drives greater plate coupling and triggers dynamic uplift of the retroarc region. Rapid uplift of the retroarc basement not only leads to disruption of the storage capacity of the basin and to cannibalization of previously deposited sediments but also generates additional detritus shed from the uplifted basement blocks. During humid or deglaciation stages, river discharge is augmented by intense rainfall or melting ice, and the increased capacity of fluvial transport leads to massive export of sediment beyond the basin and towards the ocean shores. In dry stages such as the present one, instead, fluvial discharge is drastically reduced to the point that even main rivers become endorheic (e.g. Río Abaucán and Río Desaguadero itself) and orogenic detritus is partly dumped in the retroarc basin, reworked by winds, and temporarily accumulated in dune fields.

Finally, and specifically relevant for provenance studies and their implications, the compositional signatures of terrigenous sediments accumulated in these three different types of sedimentary basins are also radically different. Foreland basins are typically filled with feldspatho-quartzo-lithic sedimentaclastic to litho-feldspatho-quartzose metamorphiclastic sand, whereas the pro-side of an Apennine-type thrust belt sheds chiefly quartzo-lithic sedimentaclastic detritus, and the retro-side of an Andean-type cordillera quartzo-feldspatho-lithic volcaniclastic to recycled litho-quartzose detritus (Garzanti et al., 2007). Such a profound difference makes provenance research a fundamental approach not only to

determine the palaeogeodynamic setting of ancient orogenic sandstone suites but also to discriminate among different types of orogenic belts and to unravel their evolution in space and time.

9 | CONCLUSIONS

Foreland basins, retroarc basins, and foredeeps are different types of sedimentary basins associated with different types of orogenic belts, made of different geological domains and consequently shedding detritus with different compositional signatures. Different geodynamic setting, subduction geometry and location (i.e. lower plate vs. upper plate) imply different applied forces, topographic relief, subsidence mechanisms, and hence drainage patterns, storage capacity and different ratio between sediment retained in the basin and sediment exported long-distance towards depositional sinks formed in even totally unrelated tectonic environments.

This sediment-provenance study is focused on central Argentina, a classic example of a broken retroarc basin where changes in subduction geometry have exerted a fundamental control on the tectonic, magmatic and sedimentary evolution of the retroarc region and on transcontinental fluvial sediment transport modulated by climate. In the Pampean flat-slab segment, comprised between 27° and 33°S and corresponding to a ca. 600-km-long magmatic gap between the Central and Southern Volcanic Zones, reduction of the subduction angle drives greater plate coupling and strong uplift of the upper plate. Extreme elevations above 6,000 m a.s.l. are, thus, reached not only within the Andean cordillera but also by strongly uplifted basement blocks of the broken retroarc basin. Rugged relief and slope instability, coupled with intense seismicity and extreme climatic events, trigger large landslides and debris flows, thus generating large amounts of sediment. Presently arid climate in the rain shadow of the Andes and structural partitioning of the retroarc basin give rise to a drainage network strongly conditioned by basement uplifts and interspersed with dune fields and saline lakes, which has changed repeatedly in response to changing climatic, tectonic and magmatic regimes through time.

Although largely derived from mesosilicic arc rocks of the cordillera, the petrographic and mineralogical signatures of detritus transported by the Desaguadero, Colorado and Negro rivers reflect significant differences in the tectonostratigraphic levels of the orogen exposed along strike, together with the different character and crystallization conditions of arc magmas through space and time. River sand, thus, changes from feldspatho-litho-quartzose or litho-feldspatho-quartzose in the north of the study region, where detritus from sedimentary and basement rocks is more common, to mostly quartzo-feldspatho-lithic in the centre and to feldspatho-lithic in the south, where volcanic detritus is overwhelming. The tHM suite also changes markedly from amphibole ≫ clinopyroxene > orthopyroxene in the north, to amphibole ≈ clinopyroxene ≈ orthopyroxene in the centre and to orthopyroxene ≥ clinopyroxene ≫ amphibole in the south. Such different signatures allow us to trace long-distance sediment dispersal pathways. Constrained by flexural upwarps and faulted blocks in the retroarc basin and by longshore currents generated by swells and storm waves at sea, the composite fluvial + littoral sediment route follows a knight's move, first eastwards across the continent and next northwards along the coast for more than 2,000 km overall.

Sediment generation and transport efficiency from source to sink strongly depend on climatic conditions. In the dry climate of today, fluvial discharge is reduced to the point that even the Río Desaguadero mainstem has become endorheic and orogenic detritus is partly dumped in the retroarc basin, where it may be reworked by winds and temporarily accumulated in dune fields. Water and sediment discharge were much higher during deglaciation and humid stages of the Pleistocene to early Holocene, when huge volumes of detritus generated from cordilleran highlands were flushed across northern Patagonia to the Atlantic Ocean, fostering one of the world's widest and smoothest continental shelves and reaching as far north as the southern mouth of the Río de la Plata estuary.

ACKNOWLEDGEMENTS

Field work has been made possible with the fundamental help of CONICET – UNLP (Centro de Investigaciones Geológicas – Universidad Nacional de la Plata) and of the exquisite courtesy of Elisa Beilinson. Much appreciated were discussions with Carlos Cingolani and colleagues at the University of La Plata, and with Carlo Doglioni, Peter DeCelles, Ray Ingersoll, Hella Wittmann and Claudio Faccenna through the years. Pablo Montilla and Liliana Tomich kindly provided sand samples from northern provinces (San Juan, La Rioja and Catamarca). Editor Peter Burgess, Andrea Di Giulio, Sarah George and Zachary Sickmann offered constructive critical advice. This study is an outcome of Progetto Dipartimenti di Eccellenza funded by MIUR 2018–2022. Open Access Funding provided by Universita degli Studi di Milano-Bicocca within the CRUI agreement.

CONFLICT OF INTEREST

The authors declare that they have no conflict of interests that could have influenced the work reported in this paper.

PEER REVIEW

The peer review history for this article is available at https://publons.com/publon/10.1111/bre.12607.

DATA AVAILABILITY STATEMENT

The data that support the findings of this study are available from the corresponding author upon request.

ORCID

Eduardo Garzanti https://orcid.org/0000-0002-8638-9322
Tomas Capaldi https://orcid.org/0000-0003-4894-736X
Giovanni Vezzoli https://orcid.org/0000-0003-2907-0283

REFERENCES

Affolter, M. D., & Ingersoll, R. V. (2019). Quantitative analysis of volcanic lithic fragments. *Journal of Sedimentary Research*, *89*(6), 479–486. https://doi.org/10.2110/jsr.2019.30

Allen, P. A., Burgess, P. M., Galewsky, J., & Sinclair, H. D. (2001). Flexural-eustatic numerical model for drowning of the Eocene perialpine carbonate ramp and implications for Alpine geodynamics. *Geological Society of America Bulletin*, *113*(8), 1052–1066. https://doi.org/10.1130/0016-7606(2001)113<1052:FENMFD>2.0.CO;2

Allmendinger, R. W., & Judge, P. A. (2014). The Argentine Precordillera: A foreland thrust belt proximal to the subducted plate. *Geosphere*, *10*(6), 1203–1218. https://doi.org/10.1130/GES01062.1

Alvarado, P., Pardo, M., Gilbert, H., Miranda, S., Anderson, M., Saez, M., & Beck, S. (2009). Flat-slab subduction and crustal models for the seismically active Sierras Pampeanas region of Argentina. In S. M. Kay, V. A. Ramos, & W. R. Dickinson (Eds.), *Backbone of the Americas: Shallow subduction, plateau uplift, and ridge and terrane collision* (Vol. *204*, pp. 261–278). Geological Society of America, Memoir.

Amadori, C., Toscani, G., Di Giulio, A., Maesano, F. E., D'Ambrogi, C., Ghielmi, M., & Fantoni, R. (2019). From cylindrical to non-cylindrical foreland basin: Pliocene-Pleistocene evolution of the Po Plain-Northern Adriatic basin (Italy). *Basin Research*, *31*(5), 991–1015. https://doi.org/10.1111/bre.12369

Amsler, M. L., Drago, E. C., & Paira, A. R. (2007). Fluvial sediments: Main channel and floodplain interrelationships. In M. H. Iriondo, J. C. Paggi & M. J. Parma (Eds.), *The Middle Paraná River: Limnology of a subtropical wetland* (pp. 123–142). Springer.

Andò, S., Morton, A., & Garzanti, E. (2014). Metamorphic grade of source rocks revealed by chemical fingerprints of detrital amphibole and garnet. In R. A. Scott, H. R. Smyth, A. C. Morton & N. Richardson (Eds.), *Sediment provenance studies in hydrocarbon exploration and production* (Vol. *386*, pp. 351–371). Geological Society of London, Special Publication.

Aragón, E., Castro, A., Díaz-Alvarado, J., & Liu, D. Y. (2011). The North Patagonian batholith at Paso Puyehue (Argentina-Chile). SHRIMP ages and compositional features. *Journal of South American Earth Sciences*, *32*(4), 547–554.

Aragón, E., Fernando, D., Cuffaro, M., Doglioni, C., Ficini, E., Pinotti, L., Nacif, S., Demartis, M., Hernando, I., & Fuentes, T. (2020). The westward lithospheric drift, its role on the subduction and transform zones surrounding Americas: Andean to cordilleran orogenic types cyclicity. *Geoscience Frontiers*, *11*(4), 1219–1229.

Audley-Charles, M. G., Curray, J. R., & Evans, G. (1977). Location of major deltas. *Geology*, *5*(6), 341–344. https://doi.org/10.1130/0091-7613(1977)5<341:LOMD>2.0.CO;2

Bahlburg, H., Vervoort, J. D., Du Frane, S. A., Bock, B., Augustsson, C., & Reimann, C. (2009). Timing of crust formation and recycling in accretionary orogens: Insights learned from the western margin of South America. *Earth-Science Reviews*, *97*(1–4), 215–241. https://doi.org/10.1016/j.earscirev.2009.10.006

Barazangi, M., & Isacks, B. L. (1976). Spatial distribution of earthquakes and subduction of the Nazca plate beneath South America. *Geology*, *4*(11), 686–692. https://doi.org/10.1130/0091-7613(1976)4<686:SDOEAS>2.0.CO;2

Bianchi, A. R., & Cravero, S. A. C. (2010). *Atlas climático digital de la República Argentina*. Instituto Nacional de Tecnología Agropecuaria.

Blasi, A. M. (1991). Sedimentología de las gravas del Río Colorado, Argentina. *Revista Del Museo De La Plata*, *10*(93), 243–264.

Blasi, A., & Manassero, M. J. (1990). The Colorado River of Argentina: Source, climate, and transport as controlling factors on sand composition. *Journal of South American Earth Sciences*, *3*(1), 65–70. https://doi.org/10.1016/0895-9811(90)90018-V

Bonetto, A. A., & Wais, I. R. (2006). Southern South American streams and rivers. In C. E. Cushing, K. W. Cummins & G. W. Minshall (Eds.), *River and stream ecosystems of the world: With a new introduction* (pp. 257–293). University of California Press.

Brunet, F., Gaiero, D., Probst, J. L., Depetris, P. J., Gauthier Lafaye, F., & Stille, P. (2005). $\delta^{13}C$ tracing of dissolved inorganic carbon sources in Patagonian rivers (Argentina). *Hydrological Processes*, *19*(17), 3321–3344.

Burbank, D. W., Beck, R. A., & Mulder, T. (1996). The Himalayan foreland basin. In A. Yin & T. M. Harrison (Eds.), *The tectonic evolution of Asia* (pp. 149–188). Cambridge University Press.

Butler, K. L., Horton, B. K., Echaurren, A., Folguera, A., & Fuentes, F. (2020). Cretaceous-Cenozoic growth of the Patagonian broken foreland basin, Argentina: Chronostratigraphic framework and provenance variations during transitions in Andean subduction dynamics. *Journal of South American Earth Sciences*, *97*, 102242. https://doi.org/10.1016/j.jsames.2019.102242

Capaldi, T. N., George, S. M. W., Hirtz, J. A., Horton, B. K., & Stockli, D. F. (2019). Fluvial and eolian sediment mixing during changing climate conditions recorded in Holocene Andean foreland deposits from Argentina (31–33°S). *Frontiers in Earth Science*, *7*, 298. https://doi.org/10.3389/feart.2019.00298

Capaldi, T. N., Horton, B. K., McKenzie, N. R., Mackaman-Lofland, C., Stockli, D. F., Ortiz, G., & Alvarado, P. (2020). Neogene retroarc foreland basin evolution, sediment provenance, and magmatism in response to flat slab subduction, western Argentina. *Tectonics*, *39*(7), e2019TC005958.

Capaldi, T. N., Horton, B. K., McKenzie, N. R., Stockli, D. F., & Odlum, M. L. (2017). Sediment provenance in contractional orogens: The detrital zircon record from modern rivers in the Andean fold-thrust belt and foreland basin of western Argentina. *Earth and Planetary Science Letters*, *479*, 83–97. https://doi.org/10.1016/j.epsl.2017.09.001

Capaldi, T. N., McKenzie, N. R., Horton, B. K., Mackaman-Lofland, C., Colleps, C. L., & Stockli, D. F. (2021). Detrital zircon record

of Phanerozoic magmatism in the southern Central Andes. *Geosphere*, *17*, 876–897. https://doi.org/10.1130/GES02346.1

Carminati, E., & Doglioni, C. (2012). Alps vs. Apennines: The paradigm of a tectonically asymmetric Earth. *Earth-Science Reviews*, *112*(1–2), 67–96.

Carretier, S., Tolorza, V., Regard, V., Aguilar, G., Bermúdez, M. A., Martinod, J., Guyot, J.-L., Hérail, G., & Riquelme, R. (2018). Review of erosion dynamics along the major NS climatic gradient in Chile and perspectives. *Geomorphology*, *300*, 45–68.

Charrier, R., Baeza, O., Elgueta, S., Flynn, J. J., Gans, P., Kay, S. M., Muñoz, N., Wyss, A. R., & Zurita, E. (2002). Evidence for Cenozoic extensional basin development and tectonic inversion south of the flat-slab segment, southern Central Andes, Chile (33–36°S.L.). *Journal of South American Earth Sciences*, *15*(1), 117–139.

Charrier, R., Ramos, V. A., Tapia, F., & Sagripanti, L. (2015). Tectono-stratigraphic evolution of the Andean Orogen between 31 and 37°S (Chile and Western Argentina). *Geological Society of London, Special Publications*, *399*(1), 13–61. https://doi.org/10.1144/SP399.20

Cibin, U., Spadafora, E., Zuffa, G. G., & Castellarin, A. (2001). Continental collision history from arenites of episutural basins in the Northern Apennines, Italy. *Geological Society of America Bulletin*, *113*(1), 4–19. https://doi.org/10.1130/0016-7606(2001)113<0004:CCHFAO>2.0.CO;2

Cingolani, C. A., & Ramos, V. A. (2017). Pre-Carboniferous tectonic evolution of the San Rafael block, Mendoza Province. In C. A. Cingolani, & C. Cingolani (Eds.), *Pre-Carboniferous evolution of the San Rafael Block, Argentina* (pp. 239–255). Springer.

Cingolani, C. A., Uriz, N., Chemale, F. Jr., & Varela, R. (2012). Las rocas monzoníticas del sector oriental del plutón de Cacheuta, Precordillera mendocina: Características geoquímicas y edad U/Pb (LA-ICP-MS). *Revista De La Asociación Geológica Argentina*, *69*(2), 195–206.

Clift, P. D., Shimizu, N., Layne, G. D., Blusztajn, J. S., Gaedicke, C., Schluter, H. U., Clark, M. K., & Amjad, S. (2001). Development of the Indus Fan and its significance for the erosional history of the Western Himalaya and Karakoram. *Geological Society of America Bulletin*, *113*(8), 1039–1051. https://doi.org/10.1130/0016-7606(2001)113<1039:DOTIFA>2.0.CO;2

Comas Cufí, M., & Thió i Fernández de Henestrosa, S. (2011). CoDaPack 2.0: A stand-alone, multi-platform compositional software.

Cortizo, L., & Isla, F. I. (2012). Dinámica de la barrera medanosa e islas de barrera de Patagones (Buenos Aires, Argentina). *Latin American Journal of Sedimentology and Basin Analysis*, *19*(1), 47–63.

Cristallini, E. O., & Ramos, V. A. (2000). Thick-skinned and thin-skinned thrusting in the La Ramada fold and thrust belt: Crustal evolution of the High Andes of San Juan, Argentina (32°S.L.). *Tectonophysics*, *317*(3–4), 205–235. https://doi.org/10.1016/S0040-1951(99)00276-0

Dahlquist, J. A., Pankhurst, R. J., Gaschnig, R. M., Rapela, C. W., Casquet, C., Alasino, P. H., Galindo, C., & Baldo, E. G. (2013). Hf and Nd isotopes in Early Ordovician to Early Carboniferous granites as monitors of crustal growth in the Proto-Andean margin of Gondwana. *Gondwana Research*, *23*(4), 1617–1630. https://doi.org/10.1016/j.gr.2012.08.013

Damanti, J. F. (1993). Geomorphic and structural controls on facies patterns and sediment composition in a modern foreland basin. In M. Marzo, & C. Puigdefábregas (Eds.), *Alluvial sedimentation* (Vol. *17*, pp. 221–233). International Association of Sedimentologists, Special Publication.

Dávila, F. M., Astini, R. A., Jordan, T. E., Gehrels, G., & Ezpeleta, M. (2007). Miocene forebulge development previous to broken foreland partitioning in the southern Central Andes, west-central Argentina. *Tectonics*, *26*(5), TC5016. https://doi.org/10.1029/2007TC002118

Dávila, F. M., & Lithgow-Bertelloni, C. (2015). Dynamic uplift during slab flattening. *Earth and Planetary Science Letters*, *425*, 34–43. https://doi.org/10.1016/j.epsl.2015.05.026

Dávila, F. M., Lithgow-Bertelloni, C., & Giménez, M. (2010). Tectonic and dynamic controls on the topography and subsidence of the Argentine Pampas: The role of the flat slab. *Earth and Planetary Science Letters*, *295*, 187–194. https://doi.org/10.1016/j.epsl.2010.03.039

De Doncker, F., Herman, F., & Fox, M. (2020). Inversion of provenance data and sediment load into spatially varying erosion rates. *Earth Surface Processes and Landforms*, *45*(15), 3879–3901. https://doi.org/10.1002/esp.5008

DeCelles, P. G. (2012). Foreland basin systems revisited: Variations in response to tectonic settings. In C. Busby & A. Azor (Eds.), *Tectonics of sedimentary basins: Recent advances* (pp. 405–426). Blackwell.

DeCelles, P. G., Carrapa, B., Horton, B. K., & Gehrels, G. E. (2011). Cenozoic foreland basin system in the central Andes of northwestern Argentina: Implications for Andean geodynamics and modes of deformation. *Tectonics*, *30*(6), TC6013. https://doi.org/10.1029/2011TC002948

DeCelles, P. G., Gehrels, G. E., Najman, Y., Martin, A. J., Carter, A., & Garzanti, E. (2004). Detrital geochronology and geochemistry of Cretaceous–Early Miocene strata of Nepal: implications for timing and diachroneity of initial Himalayan orogenesis. *Earth and Planetary Science Letters*, *227*, 313–330. https://doi.org/10.1016/j.epsl.2004.08.019

DeCelles, P. G., & Giles, K. A. (1996). Foreland basin systems. *Basin Research*, *8*(2), 105–123. https://doi.org/10.1046/j.1365-2117.1996.01491.x

DeCelles, P. G., & Horton, B. K. (2003). Early to middle Tertiary foreland basin development and the history of Andean crustal shortening in Bolivia. *Geological Society of America Bulletin*, *115*(1), 58–77. https://doi.org/10.1130/0016-7606(2003)115<0058:ETMTFB>2.0.CO;2

del Río, J. L., Colado, U. R., & Gaido, E. S. (1991). Estabilidad y dinámica del delta de reflujo de la boca del Río Negro. *Revista De La Asociación Geológica Argentina*, *46*(3–4), 325–332.

Deruelle, B. (1982). Petrology of the Plio-Quaternary volcanism of the south-central and meridional Andes. *Journal of Volcanology and Geothermal Research*, *14*(1–2), 77–124. https://doi.org/10.1016/0377-0273(82)90044-0

Dèzes, P., Schmid, S. M., & Ziegler, P. A. (2004). Evolution of the European Cenozoic Rift System: Interaction of the Alpine and Pyrenean orogens with their foreland lithosphere. *Tectonophysics*, *389*(1–2), 1–33. https://doi.org/10.1016/j.tecto.2004.06.011

Di Giulio, A., Ronchi, A., Sanfilippo, A., Balgord, E. A., Carrapa, B., & Ramos, V. A. (2017). Cretaceous evolution of the Andean margin between 36° S and 40°S latitude through a multi-proxy provenance analysis of Neuquén Basin strata (Argentina). *Basin Research*, *29*(3), 284–304. https://doi.org/10.1111/bre.12176

Di Giulio, A., Ronchi, A., Sanfilippo, A., Tiepolo, M., Pimentel, M., & Ramos, V. A. (2012). Detrital zircon provenance from the

Neuquén Basin (south-central Andes): Cretaceous geodynamic evolution and sedimentary response in a retroarc-foreland basin. *Geology*, *40*(6), 559–562. https://doi.org/10.1130/G33052.1

Dickinson, W. R. (1970). Interpreting detrital modes of graywacke and arkose. *Journal of Sedimentary Research*, *40*(2), 695–707.

Dickinson, W. R. (1988). Provenance and sediment dispersal in relation to paleotectonics and paleogeography of sedimentary basins. In K. L. Kleinspehn & C. Paola (Eds.), *New perspectives in basin analysis* (pp. 3–25). Springer.

Doglioni, C. (1994). Foredeeps versus subduction zones. *Geology*, *22*(3), 271–274. https://doi.org/10.1130/0091-7613(1994)022<0271:FVSZ>2.3.CO;2

Doglioni, C., Carminati, E., Cuffaro, M., & Scrocca, D. (2007). Subduction kinematics and dynamic constraints. *Earth-Science Reviews*, *83*(3–4), 125–175. https://doi.org/10.1016/j.earscirev.2007.04.001

Doglioni, C., Gueguen, E., Harabaglia, P., & Mongelli, F. (1999). On the origin of west-directed subduction zones and applications to the western Mediterranean. *Geological Society, London, Special Publications*, *156*(1), 541–561. https://doi.org/10.1144/GSL.SP.1999.156.01.24

Doglioni, C., Harabaglia, P., Merlini, S., Mongelli, F., Peccerillo, A. T., & Piromallo, C. (1999). Orogens and slabs vs. their direction of subduction. *Earth-Science Reviews*, *45*(3–4), 167–208. https://doi.org/10.1016/S0012-8252(98)00045-2

Doglioni, C., & Panza, G. (2015). Polarized plate tectonics. *Advances in Geophysics*, *56*, 1–167.

Einsele, G., Ratschbacher, L., & Wetzel, A. (1996). The Himalaya-Bengal Fan denudation-accumulation system during the past 20 Ma. *The Journal of Geology*, *104*(2), 163–184. https://doi.org/10.1086/629812

Eppinger, K. J., & Rosenfeld, U. (1996). Western margin and provenance of sediments of the Neuquén Basin (Argentina) in the Late Jurassic and Early Cretaceous. *Tectonophysics*, *259*(1–3), 229–244. https://doi.org/10.1016/0040-1951(95)00157-3

Farías, M., Charrier, R., Carretier, S., Martinod, J., Fock, A., Campbell, D., Cáceres, J., & Comte, D. (2008). Late Miocene high and rapid surface uplift and its erosional response in the Andes of central Chile (33°–35°S). *Tectonics*, *27*, TC1005. https://doi.org/10.1029/2006TC002046

Figuereido, J., Hoorn, C., Van der Ven, P., & Soares, E. (2009). Late Miocene onset of the Amazon River and the Amazon deep-sea fan: Evidence from the Foz do Amazonas Basin. *Geology*, *37*(7), 619–622. https://doi.org/10.1130/G25567A.1

Folguera, A., Naranjo, J. A., Orihashi, Y., Sumino, H., Nagao, K., Polanco, E., & Ramos, V. A. (2009). Retroarc volcanism in the northern San Rafael Block (34–35 30′S), southern Central Andes: Occurrence, age, and tectonic setting. *Journal of Volcanology and Geothermal Research*, *186*(3–4), 169–185. https://doi.org/10.1016/j.jvolgeores.2009.06.012

Folguera, A., & Ramos, V. A. (2011). Repeated eastward shifts of arc magmatism in the Southern Andes: A revision to the long-term pattern of Andean uplift and magmatism. *Journal of South American Earth Sciences*, *32*(4), 531–546. https://doi.org/10.1016/j.jsames.2011.04.003

Folguera, A., Zárate, M., Tedesco, A., Dávila, F., & Ramos, V. A. (2015). Evolution of the Neogene Andean foreland basins of the Southern Pampas and northern Patagonia (34°–41°S), Argentina. *Journal of South American Earth Sciences*, *64*, 452–466. https://doi.org/10.1016/j.jsames.2015.05.010

Fosdick, J. C., Carrapa, B., & Ortíz, G. (2015). Faulting and erosion in the Argentine Precordillera during changes in subduction regime: Reconciling bedrock cooling and detrital records. *Earth and Planetary Science Letters*, *432*, 73–83. https://doi.org/10.1016/j.epsl.2015.09.041

France-Lanord, C., Spiess, V., Klaus, A., & Schwenk, T.; Expedition 354 Scientists. (2016). Expedition 354 summary. In C. France-Lanord, T. Schwenk & A. Klaus (Eds.), *Expedition 354 scientific prospectus: Bengal Fan* (Vol. *354*, pp. 1–35). Proceedings of the International Ocean Discovery Program. International Ocean Discovery Program. https://doi.org/10.14379/iodp.proc.354.101.2016

Franke, D., Neben, S., Schreckenberger, B., Schulze, A., Stiller, M., & Krawczyk, C. M. (2006). Crustal structure across the Colorado Basin, offshore Argentina. *Geophysical Journal International*, *165*(3), 850–864. https://doi.org/10.1111/j.1365-246X.2006.02907.x

Fuentes, F., Horton, B. K., Starck, D., & Boll, A. (2016). Structure and tectonic evolution of hybrid thick-and thin-skinned systems in the Malargüe fold–thrust belt, Neuquén basin, Argentina. *Geological Magazine*, *153*(5–6), 1066–1084. https://doi.org/10.1017/S0016756816000583

Gabriel, K. R. (1971). The biplot graphic display of matrices with application to principal component analysis. *Biometrika*, *58*(3), 453–467. https://doi.org/10.1093/biomet/58.3.453

Gallay, M., Martinez, J. M., Mora, A., Castellano, B., Yépez, S., Cochonneau, G., Alfonso, J. A., Carrera, J. M., López, J. L., & Laraque, A. (2019). Assessing Orinoco river sediment discharge trend using MODIS satellite images. *Journal of South American Earth Sciences*, *91*, 320–331. https://doi.org/10.1016/j.jsames.2019.01.010

Garzanti, E. (2017). The maturity myth in sedimentology and provenance analysis. *Journal of Sedimentary Research*, *87*(4), 353–365. https://doi.org/10.2110/jsr.2017.17

Garzanti, E. (2019). Petrographic classification of sand and sandstone. *Earth-Science Reviews*, *192*, 545–563. https://doi.org/10.1016/j.earscirev.2018.12.014

Garzanti, E. (2020). The Himalayan Foreland Basin from collision onset to the present: A sedimentary–petrology perspective. In P. J. Treloar & M. P. Searle (Eds.), *Himalayan tectonics: A modern synthesis* (Vol. *483*, pp. 65–122). Geological Society of London, Special Publication.

Garzanti, E., & Andò, S. (2007). Heavy mineral concentration in modern sands: implications for provenance interpretation. In M. Mange & D. Wright (Eds.), *Heavy minerals in use* (Vol. *58*, pp. 517–545). Elsevier, Amsterdam, Developments in Sedimentology.

Garzanti, E., & Andò, S. (2019). Heavy minerals for junior woodchucks. In S. Andò (Ed.), *Heavy minerals: Methods & case histories* (Vol. *9*(3), p. 148). MDPI, Basel, Minerals. https://doi.org/10.3390/min9030148

Garzanti, E., Doglioni, C., Vezzoli, G., & Ando, S. (2007). Orogenic belts and orogenic sediment provenance. *The Journal of Geology*, *115*(3), 315–334. https://doi.org/10.1086/512755

Garzanti, E., Limonta, M., Vezzoli, G., & Sosa, N. (2021). From Patagonia to Río de la Plata: Multistep long-distance littoral transport of Andean volcaniclastic sand along the Argentine passive margin. *Sedimentology*, in press. https://doi.org/10.1111/sed.12902

Garzanti, E., & Malusà, M. G. (2008). The Oligocene Alps: Domal unroofing and drainage development during early orogenic

growth. *Earth and Planetary Science Letters*, *268*(3–4), 487–500. https://doi.org/10.1016/j.epsl.2008.01.039

Garzanti, E., Resentini, A., Vezzoli, G., Andò, S., Malusà, M., & Padoan, M. (2012). Forward compositional modelling of Alpine orogenic sediments. *Sedimentary Geology*, *280*, 149–164. https://doi.org/10.1016/j.sedgeo.2012.03.012

Garzanti, E., Vermeesch, P., Padoan, M., Resentini, A., Vezzoli, G., & Andò, S. (2014). Provenance of passive-margin sand (Southern Africa). *The Journal of Geology*, *122*(1), 17–42. https://doi.org/10.1086/674803

Garzanti, E., & Vezzoli, G. (2003). A classification of metamorphic grains in sands based on their composition and grade. *Journal of Sedimentary Research*, *73*(5), 830–837. https://doi.org/10.1306/012203730830

Garzanti, E., Vezzoli, G., & Andò, S. (2011). Paleogeographic and paleodrainage changes during Pleistocene glaciations (Po Plain, northern Italy). *Earth-Science Reviews*, *105*(1–2), 25–48. https://doi.org/10.1016/j.earscirev.2010.11.004

Garzanti, E., Vezzoli, G., Ando, S., & Castiglioni, G. (2001). Petrology of rifted-margin sand (Red Sea and Gulf of Aden, Yemen). *The Journal of Geology*, *109*(3), 277–297. https://doi.org/10.1086/319973

Geological Map of South America. (2019). Scale: 1:5,000,000. In J. Gómez, C. Schobbenhaus & N. E. Montes (Eds.), *Commission for the geological map of the world (CGMW)*. Colombian Geological Survey and Geological Survey of Brazil.

Giambiagi, L., Mescua, J., Bechis, F., Tassara, A., & Hoke, G. (2012). Thrust belts of the southern Central Andes: Along-strike variations in shortening, topography, crustal geometry, and denudation. *Geological Society of America Bulletin*, *124*(7–8), 1339–1351. https://doi.org/10.1130/B30609.1

Giambiagi, L. B., Mescua, J. F., Heredia, N., Farías, P., García Sansegundo, J., Fernández, C., Stier, S., Pérez, D., Bechis, F., Moreiras, S. M., & Lossada, A. C. (2014). Reactivation of Paleozoic structures during Cenozoic deformation in the Cordón del Plata and Southern Precordillera ranges (Mendoza, Argentina). *Journal of Iberian Geology*, *40*(2), 309–320. https://doi.org/10.5209/rev_JIGE.2014.v40.n2.45302

Gianni, G. M., Dávila, F. M., Echaurren, A., Fennell, L., Tobal, J., Navarrete, C., Quezada, P., Folguera, A., & Giménez, M. (2018). A geodynamic model linking Cretaceous orogeny, arc migration, foreland dynamic subsidence and marine ingression in southern South America. *Earth-Science Reviews*, *185*, 437–462. https://doi.org/10.1016/j.earscirev.2018.06.016

Gianni, G. M., García, H. P., Lupari, M., Pesce, A., & Folguera, A. (2017). Plume overriding triggers shallow subduction and orogeny in the southern Central Andes. *Gondwana Research*, *49*, 387–395. https://doi.org/10.1016/j.gr.2017.06.011

Gill, J. (1981). *Orogenic andesites and plate tectonics* (p. 390). Springer.

Gonzalez, M., Clavel, F., Christiansen, R., Gianni, G. M., Klinger, F. L., Martinez, P., Butler, K., Suriano, J., Mardonez, D., & Díaz, M. (2020). The Iglesia basin in the southern Central Andes: A record of backarc extension before wedge-top deposition in a foreland basin. *Tectonophysics*, *792*, 228590. https://doi.org/10.1016/j.tecto.2020.228590

Graham, S. A., Dickinson, W. R., & Ingersoll, R. V. (1975). Himalayan-Bengal model for flysch dispersal in the Appalachian-Ouachita system. *Geological Society of America Bulletin*, *86*(3), 273–286.

Haschke, M., Günther, A., Melnick, D., Echtler, H., Reutter, K. J., Scheuber, E., & Oncken, O. (2006). Central and southern Andean tectonic evolution inferred from arc magmatism. In O. Oncken (Ed.), *The Andes* (pp. 337–353). Springer.

Hermanns, R. L., Fauqué, L., & Wilson, C. G. (2015). ^{36}Cl terrestrial cosmogenic nuclide dating suggests Late Pleistocene to Early Holocene mass movements on the south face of Aconcagua mountain and in the Las Cuevas–Horcones valleys, Central Andes, Argentina. In S. A. Sepúlveda, L. B. Giambiagi, S. M. Moreiras, L. Pinto, M. Tunik, G. D. Hoke & M. Farías (Eds.), *Geodynamic processes in the Andes of Central Chile and Argentina* (Vol. *399*, pp. 345–368). Geological Society of London, Special Publication.

Hervé, F., Fanning, C. M., Calderón, M., & Mpodozis, C. (2014). Early Permian to Late Triassic batholiths of the Chilean Frontal Cordillera (28°–31°S): SHRIMP U-Pb zircon ages and Lu–Hf and O isotope systematics. *Lithos*, *184*, 436–446. https://doi.org/10.1016/j.lithos.2013.10.018

Hinderer, M. (2012). From gullies to mountain belts: A review of sediment budgets at various scales. *Sedimentary Geology*, *280*, 21–59. https://doi.org/10.1016/j.sedgeo.2012.03.009

Horton, B. K. (2018). Tectonic regimes of the central and southern Andes: Responses to variations in plate coupling during subduction. *Tectonics*, *37*(2), 402–429. https://doi.org/10.1002/2017TC004624

Horton, B. K., Fuentes, F., Boll, A., Starck, D., Ramirez, S. G., & Stockli, D. F. (2016). Andean stratigraphic record of the transition from backarc extension to orogenic shortening: A case study from the northern Neuquén Basin, Argentina. *Journal of South American Earth Sciences*, *71*, 17–40. https://doi.org/10.1016/j.jsames.2016.06.003

Howell, J. A., Schwarz, E., Spalletti, L. A., & Veiga, G. D. (2005). The Neuquén basin: An overview. In G. D. Veiga, L. A. Spalletti, J. A. Howell & E. Schwarz (Eds.), *The Neuquén basin, Argentina: A case study in sequence stratigraphy and basin dynamics* (Vol. *252*, pp. 1–14). Geological Society of London, Special Publication.

Hu, X. M., Garzanti, E., Li, J., BouDagher-Fadel, M., Coletti, G., Ma, A., Liang, W., & Xue, W. W. The "underfilled trinity" from the western Alpine foreland basin: Reality or myth? *Tectonics*, in review.

Hubert, J. F. (1962). A zircon-tourmaline-rutile maturity index and the interdependence of the composition of heavy mineral assemblages with the gross composition and texture of sandstones. *Journal of Sedimentary Petrology*, *32*(3), 440–450.

Ingersoll, R. V., Bullard, T. F., Ford, R. L., Grimm, J. P., Pickle, J. D., & Sares, S. W. (1984). The effect of grain size on detrital modes: A test of the Gazzi-Dickinson point-counting method. *Journal of Sedimentary Petrology*, *54*(1), 103–116.

Introcaso, A., & Ruiz, F. (2001). Geophysical indicators of Neogene strike-slip faulting in the Desaguadero-Bermejo tectonic lineament (northwestern Argentina). *Journal of South American Earth Sciences*, *14*(7), 655–663. https://doi.org/10.1016/S0895-9811(01)00057-8

Iriondo, M. (1994). Los climas cuaternarios de la región pampeana. *Museo Provincial De Ciencias Naturales" Florentino Ameghino"*, *4*(2), 48.

Iriondo, M. (1999). Climatic changes in the South American plains: Records of a continent-scale oscillation. *Quaternary International*, *57*, 93–112. https://doi.org/10.1016/S1040-6182(98)00053-6

Iriondo, M. H., & García, N. O. (1993). Climatic variations in the Argentine plains during the last 18,000 years. *Palaeogeography,*

Palaeoclimatology, Palaeoecology, *101*(3–4), 209–220. https://doi.org/10.1016/0031-0182(93)90013-9

Isla, F. I. (2014). Variaciones espaciales y temporales de la deriva litoral, SE de la Provincia de Buenos Aires, Argentina. *Revista Geográfica Del Sur*, *5*(8), 24–41.

Isla, F. I., & Cortizo, L. C. (2014). Sediment input from fluvial sources and cliff erosion to the continental shelf of Argentina. *Revista De Gestão Costeira Integrada-Journal of Integrated Coastal Zone Management*, *14*(4), 541–552. https://doi.org/10.5894/rgci436

Isla, F. I., Cortizo, L., Merlotto, A., Bértola, G., Albisetti, M. P., & Finocchietti, C. (2018). Erosion in Buenos Aires province: Coastal-management policy revisited. *Ocean & Coastal Management*, *156*, 107–116. https://doi.org/10.1016/j.ocecoaman.2017.09.008

Isla, F. I., Cortizo, L. C., & Orellano, H. A. T. (2001). Dinámica y evolución de las barreras medanosas, Provincia de Buenos Aires, Argentina. *Revista Brasileira De Geomorfologia*, *2*(1), 73–83.

Johnson, N. M., Jordan, T. E., Johnsson, P. A., & Naeser, C. W. (1986). Magnetic polarity stratigraphy, age and tectonic setting of fluvial sediments in an eastern Andean foreland basin, San Juan Province, Argentina. In P. A. Allen & P. Homewood (Eds.), *Foreland basins* (pp. 63–75). The International Association of Sedimentologists.

Jones, R. E., Kirstein, L. A., Kasemann, S. A., Litvak, V. D., Poma, S., Alonso, R. N., & Hinton, R. (2016). The role of changing geodynamics in the progressive contamination of Late Cretaceous to Late Miocene arc magmas in the southern Central Andes. *Lithos*, *262*, 169–191. https://doi.org/10.1016/j.lithos.2016.07.002

Jordan, T. E. (1995). Retroarc foreland and related basins. In C. J. Busby & R. V. Ingersoll (Eds.), *Tectonics of sedimentary basins* (pp. 331–362). Blackwell.

Jordan, T. E., Allmendinger, R. W., Damanti, J. F., & Drake, R. E. (1993). Chronology of motion in a complete thrust belt: The Precordillera, 30–31°S, Andes Mountains. *The Journal of Geology*, *101*(2), 135–156. https://doi.org/10.1086/648213

Jordan, T. E., Isacks, B. L., Allmendinger, R. W., Brewer, J. A., Ramos, V. A., & Ando, C. J. (1983). Andean tectonics related to geometry of subducted Nazca plate. *Geological Society of America Bulletin*, *94*(3), 341–361. https://doi.org/10.1130/0016-7606(1983)94<341:ATRTGO>2.0.CO;2

Jordan, T. E., Schlunegger, F., & Cardozo, N. (2001). Unsteady and spatially variable evolution of the Neogene Andean Bermejo foreland basin, Argentina. *Journal of South American Earth Sciences*, *14*(7), 775–798. https://doi.org/10.1016/S0895-9811(01)00072-4

Kay, S. M., Ardolino, A. A., Gorring, M. L., & Ramos, V. A. (2007). The Somuncurá Large Igneous Province in Patagonia: Interaction of a transient mantle thermal anomaly with a subducting slab. *Journal of Petrology*, *48*(1), 43–77.

Kay, S. M., Burns, W. M., Copeland, P., & Mancilla, O. (2006). Upper Cretaceous to Holocene magmatism and evidence for transient Miocene shallowing of the Andean subduction zone under the northern Neuquén Basin. In S. M. Kay & V. A. Ramos (Eds.), *Evolution of an Andean margin: A tectonic and magmatic view from the Andes* (Vol. *407*, pp. 19–60). Geological Society of America, Special Paper.

Kay, S. M., & Copeland, P. (2006). Early to middle Miocene backarc magmas of the Neuquén Basin: Geochemical consequences of slab shallowing and the westward drift of South America. In S. M. Kay & V. A. Ramos (Eds.), *Evolution of an Andean margin: A tectonic and magmatic view from the Andes to the Neuquén Basin (35°–39°S lat)* (Vol. *407*, pp. 185–213). Geological Society of America, Special Paper, https://doi.org/10.1130/2006.2407(09

Kay, S. M., Godoy, E., & Kurtz, A. (2005). Episodic arc migration, crustal thickening, subduction erosion, and magmatism in the south-central Andes. *Geological Society of America Bulletin*, *117*(1–2), 67–88. https://doi.org/10.1130/B25431.1

Kay, S. M., Mpodozis, C., Ramos, V. A., & Munizaga, F. (1991). Magma source variations for mid-late Tertiary magmatic rocks associated with a shallowing subduction zone and a thickening crust in the central Andes (28 to 33°S). In R. S. Harmon & C. W. Rapela (Eds.), *Andean magmatism and its tectonic setting* (Vol. *265*, pp. 113–137). Geological Society of America, Special Paper.

Kleiman, L. E., & Japas, M. S. (2009). The Choiyoi volcanic province at 34°S–36°S (San Rafael, Mendoza, Argentina): Implications for the Late Palaeozoic evolution of the southwestern margin of Gondwana. *Tectonophysics*, *473*(3–4), 283–299. https://doi.org/10.1016/j.tecto.2009.02.046

Kuhlemann, J., Frisch, W., Székely, B., Dunkl, I., & Kazmer, M. (2002). Post-collisional sediment budget history of the Alps: Tectonic versus climatic control. *International Journal of Earth Sciences*, *91*(5), 818–837. https://doi.org/10.1007/s00531-002-0266-y

Latrubesse, E. M., & Restrepo, J. D. (2014). Sediment yield along the Andes: Continental budget, regional variations, and comparisons with other basins from orogenic mountain belts. *Geomorphology*, *216*, 225–233. https://doi.org/10.1016/j.geomorph.2014.04.007

Le Pera, E., & Morrone, C. (2020). The use of mineral interfaces in sand-sized volcanic rock fragments to infer mechanical durability. *Journal of Palaeogeography*, *9*(21), 1–26. https://doi.org/10.1186/s42501-020-00068-8

Leanza, H. A., Hugo, C. A., & Repol, D. (2001). *Hoja Geológica 3969-I, Zapala* (Vol. *275*, pp. 1–128). Provincia del Neuquén. Instituto de Geología y Recursos Minerales, Boletín Servicio Geológico Minero Argentino, Buenos Aires.

Limonta, M., Garzanti, E., Resentini, A., Andò, S., Boni, M., & Bechstädt, T. (2015). Multicyclic sediment transfer along and across convergent plate boundaries (Barbados, Lesser Antilles). *Basin Research*, *27*(6), 696–713. https://doi.org/10.1111/bre.12095

Litvak, V. D., Spagnuolo, M. G., Folguera, A., Poma, S., Jones, R. E., & Ramos, V. A. (2015). Late Cenozoic calc-alkaline volcanism over the Payenia shallow subduction zone, South-Central Andean back-arc (34°30′–37°S), Argentina. *Journal of South American Earth Sciences*, *64*, 365–380. https://doi.org/10.1016/j.jsames.2015.09.010

Lossada, A. C., Giambiagi, L., Hoke, G., Mescua, J., Suriano, J., & Mazzitelli, M. (2018). Cenozoic uplift and exhumation of the frontal cordillera between 30° and 35°S and the influence of the subduction dynamics in the flat slab subduction Context, South Central Andes. In A. Folguera (Ed.), *The evolution of the Chilean-Argentinean Andes* (pp. 387–409). Springer.

Lupker, M., France-Lanord, C., Lavé, J., Bouchez, J., Galy, V., Métivier, F., Gaillardet, J., Lartiges, B., & Mugnier, J.-L. (2011). A Rouse-based method to integrate the chemical composition of river sediments: Application to the Ganga basin. *Journal of Geophysical Research*, *116*, F04012. https://doi.org/10.1029/2010JF001947

Mackaman-Lofland, C., Horton, B. K., Fuentes, F., Constenius, K. N., & Stockli, D. F. (2019). Mesozoic to Cenozoic retroarc basin evolution during changes in tectonic regime, southern Central

Andes (31–33°S): Insights from zircon U-Pb geochronology. *Journal of South American Earth Sciences*, *89*, 299–318. https://doi.org/10.1016/j.jsames.2018.10.004

Markert, B., Pedrozo, F., Geller, W., Friese, K., Korhammer, S., Baffico, G., Diaz, M., & Wölfl, S. (1997). A contribution to the study of the heavy-metal and nutritional element status of some lakes in the southern Andes of Patagonia (Argentina). *Science of the Total Environment*, *206*(1), 1–15. https://doi.org/10.1016/S0048-9697(97)00218-0

Marsaglia, K. M., & Ingersoll, R. V. (1992). Compositional trends in arc-related, deep-marine sand and sandstone: A reassessment of magmatic-arc provenance. *Geological Society of America Bulletin*, *104*(12), 1637–1649. https://doi.org/10.1130/0016-7606(1992)104<1637:CTIARD>2.3.CO;2

Martin, E. L., Collins, W. J., & Spencer, C. J. (2020). Laurentian origin of the Cuyania suspect terrane, western Argentina, confirmed by Hf isotopes in zircon. *Geological Society of America Bulletin*, *132*(1–2), 273–290. https://doi.org/10.1130/B35150.1

Martínez, O. A., & Kutschker, A. (2011). The 'Rodados Patagónicos' (Patagonian shingle formation) of eastern Patagonia: Environmental conditions of gravel sedimentation. *Biological Journal of the Linnean Society*, *103*, 336–345. https://doi.org/10.1111/j.1095-8312.2011.01651.x

Melo, W. D., Schillizzi, R., Perillo, G. M., & Piccolo, M. C. (2003). Influencia del área continental pampeana en la evolución morfológica del estuario de Bahía Blanca. *Latin American Journal of Sedimentology and Basin Analysis*, *10*(1), 39–52.

Milliman, J. D., & Farnsworth, K. L. (2011). *River discharge to the coastal ocean: A global synthesis* (p. 384). Cambridge University Press.

Moreiras, S. M., & Sepúlveda, S. A. (2015). Megalandslides in the Andes of central Chile and Argentina (32°–34° S) and potential hazards. In S. A. Sepúlveda, L. B. Giambiagi, S. M. Moreiras, L. Pinto, M. Tunik, G. D. Hoke & M. Farías (Eds.), *Geodynamic processes in the Andes of Central Chile and Argentina* (Vol. *399*, pp. 329–344). Geological Society of London, Special Publication.

Moreiras, S. M., Sepúlveda, S. A., Correas-González, M., Lauro, C., Vergara, I., Jeanneret, P., Junquera-Torrado, S., Cuevas, J. G., Maldonado, A., Antinao, J. L., & Lara, M. (2021). Debris flows occurrence in the semiarid central Andes under climate change scenario. *Geosciences*, *11*(2), 43, 1–25. https://doi.org/10.3390/geosciences11020043

Moreno, J. A., Dahlquist, J. A., Cámera, M. M. M., Alasino, P. H., Larrovere, M. A., Basei, M. A., Galindo, C., Zandomeni, P. S., & Rocher, S. (2020). Geochronology and geochemistry of the Tabaquito batholith (Frontal Cordillera, Argentina): Geodynamic implications and temporal correlations in the SW Gondwana margin. *Journal of the Geological Society of London*, *177*(3), 455–474.

Mpodozis, C., & Kay, S. M. (1992). Late Paleozoic to Triassic evolution of the Gondwana margin: Evidence from Chilean Frontal Cordilleran batholiths (28°S to 31°S). *Geological Society of America Bulletin*, *104*(8), 999–1014. https://doi.org/10.1130/0016-7606(1992)104<0999:LPTTEO>2.3.CO;2

Mpodozis, C., & Ramos, V. (1989). The Andes of Chile and Argentina. In G. E. Ericksen, M. T. Cañas Pinochet & J. A. Reinemund (Eds.), *Geology of the Andes and its relation to hydrocarbon and mineral resources* (Vol. *11*, Ch. 5, pp. 59–90). Circum-Pacific Council for Energy and Mineral Resources, Houston, Texas, Earth Science Series.

Naylor, M., & Sinclair, H. D. (2008). Pro-vs. retro-foreland basins. *Basin Research*, *20*(3), 285–303. https://doi.org/10.1111/j.1365-2117.2008.00366.x

Nelson, D. A., & Cottle, J. M. (2019). Tracking voluminous Permian volcanism of the Choiyoi Province into central Antarctica. *Lithosphere*, *11*(3), 386–398. https://doi.org/10.1130/L1015.1

Nivière, B., Messager, G., Carretier, S., & Lacan, P. (2013). Geomorphic expression of the southern Central Andes forebulge (37°S, Argentina). *Terra Nova*, *25*(5), 361–367. https://doi.org/10.1111/ter.12044

Ori, G. G., & Friend, P. F. (1984). Sedimentary basins formed and carried piggyback on active thrust sheets. *Geology*, *12*(8), 475–478. https://doi.org/10.1130/0091-7613(1984)12<475:SBFACP>2.0.CO;2

Pankhurst, R. J., & Rapela, C. R. (1995). Production of Jurassic rhyolite by anatexis of the lower crust of Patagonia. *Earth and Planetary Science Letters*, *134*(1–2), 23–36. https://doi.org/10.1016/0012-821X(95)00103-J

Pankhurst, R. J., Weaver, S. D., Hervé, F., & Larrondo, P. (1999). Mesozoic-Cenozoic evolution of the North Patagonian batholith in Aysen, southern Chile. *Journal of the Geological Society of London*, *156*(4), 673–694. https://doi.org/10.1144/gsjgs.156.4.0673

Parada, M. A., Nyström, J. O., & Levi, B. (1999). Multiple sources for the Coastal Batholith of central Chile (31–34°S): Geochemical and Sr–Nd isotopic evidence and tectonic implications. *Lithos*, *46*(3), 505–521. https://doi.org/10.1016/S0024-4937(98)00080-2

Parada, M. A., Rivano, S., Sepúlveda, P., Hervé, M., Hervé, F., Puig, A., Munizaga, F., Brook, M., Pankhurst, R., & Snelling, N. (1988). Mesozoic and Cenozoic plutonic development in the Andes of central Chile (30°30′–32°30′S). *Journal of South American Earth Sciences*, *1*(3), 249–260. https://doi.org/10.1016/0895-9811(88)90003-X

Perillo, G. M. E., Piccolo, M. C., Parodi, E., & Freije, R. H. (2001). The Bahía Blanca Estuary, Argentina. In U. Seeliger & B. Kjerfve (Eds.), *Coastal marine ecosystems of Latin America* (pp. 205–217). Springer.

Piccolo, M. C., & Perillo, G. M. E. (1999). The Argentina estuaries: A review. In G. M. E. Perillo (Ed.), *Estuaries of South America* (pp. 101–132). Springer.

Pinto, L., Alarcón, P., Morton, A., & Naipauer, M. (2018). Geochemistry of heavy minerals and U-Pb detrital zircon geochronology in the Manantiales Basin: Implications for Frontal Cordillera uplift and foreland basin connectivity in the Andes of central Argentina. *Palaeogeography, Palaeoclimatology, Palaeoecology*, *492*, 104–125. https://doi.org/10.1016/j.palaeo.2017.12.017

Ponce, J. F., Rabassa, J., Coronato, A., & Borromei, A. M. (2011). Palaeogeographical evolution of the Atlantic coast of Pampa and Patagonia from the last glacial maximum to the Middle Holocene. *Biological Journal of the Linnean Society*, *103*(2), 363–379. https://doi.org/10.1111/j.1095-8312.2011.01653.x

Porras, H., Pinto, L., Tunik, M., Giambiagi, L., & Deckart, K. (2016). Provenance of the Miocene Alto Tunuyán Basin (33 40′S, Argentina) and its implications for the evolution of the Andean Range: Insights from petrography and U-Pb LA–ICPMS zircon ages. *Tectonophysics*, *690*, 298–317. https://doi.org/10.1016/j.tecto.2016.09.034

Potter, P. E. (1978). Significance and origin of big rivers. *The Journal of Geology*, *86*(1), 13–33. https://doi.org/10.1086/649653

Potter, P. E. (1984). South American modern beach sand and plate tectonics. *Nature*, *311*(5987), 645–648.

Potter, P. E. (1994). Modern sands of South America: Composition, provenance and global significance. *Geologische Rundschau*, *83*(1), 212–232. https://doi.org/10.1007/BF00211904

Potter, P. E. (1997). The Mesozoic and Cenozoic paleodrainage of South America: A natural history. *Journal of South American Earth Sciences*, *10*(5–6), 331–344. https://doi.org/10.1016/S0895-9811(97)00031-X

Ramos, M. E., Folguera, A., Fennell, L., Giménez, M., Litvak, V. D., Dzierma, Y., & Ramos, V. A. (2014). Tectonic evolution of the North Patagonian Andes from field and gravity data (39–40°S). *Journal of South American Earth Sciences*, *51*, 59–75. https://doi.org/10.1016/j.jsames.2013.12.010

Ramos, V. A. (1988). The tectonics of the Central Andes; 30° to 33°S latitude. In S. P. Clark, B. C. Burchfiel & J. Suppe (Eds.), *Processes in continental lithospheric deformation* (Vol. *218*, pp. 31–54). Geological Society of America, Special Paper.

Ramos, V. A. (2009). Anatomy and global context of the Andes: Main geologic features and the Andean orogenic cycle. In S. M. Kay, V. A. Ramos & W. R. Dickinson (Eds.), *Backbone of the Americas: Shallow subduction, plateau uplift, and ridge and terrane collision* (Vol. *204*, pp. 31–65). Geological Society of America Memoir. https://doi.org/10.1130/2009.1204(02

Ramos, V. A., Cristallini, E. O., & Pérez, D. J. (2002). The Pampean flat-slab of the Central Andes. *Journal of South American Earth Sciences*, *15*(1), 59–78.

Ramos, V. A., & de Brodtkorb, M. K. (1990). The barite and celestite metallotects of the Neuquén retroarc basin, Central Argentina. In G. C. Amstutz, M. Cardozo, E. Cedillo, L. Fontboté & J. Frutos (Eds.), *Stratabound ore deposits in the Andes* (Vol. *47*, pp. 599–613), Springer.

Ramos, V. A., & Folguera, A. (2005). Tectonic evolution of the Andes of Neuquén: Constraints derived from the magmatic arc and foreland deformation. In G. D. Veiga, L. A. Spalletti, J. A. Howell & E. Schwarz (Eds.), *The Neuquén basin, Argentina: A case study in sequence stratigraphy and basin dynamics* (Vol. *252*, pp. 15–35). Geological Society of London, Special Publication.

Ramos, V. A., & Folguera, A. (2009). Andean flat-slab subduction through time. In J. B. Murphy, J. D. Keppie & A. J. Hynes (Eds.), *Ancient orogens and modern analogues* (Vol. *327*, pp. 31–54). Geological Society of London, Special Publication.

Ramos, V. A., & Folguera, A. (2011). Payenia volcanic province in the Southern Andes: An appraisal of an exceptional Quaternary tectonic setting. *Journal of Volcanology and Geothermal Research*, *201*(1–4), 53–64. https://doi.org/10.1016/j.jvolgeores.2010.09.008

Ramos, V. A., Jordan, T. E., Allmendinger, R. W., Kay, S. M., Cortés, J. M., & Palma, M. A. (1984). Chilenia: Un terreno alóctono en la evolución paleozoica de los Andes Centrales. In *Congreso Geológico Argentino* (Vol. *9*, Actas II, pp. 84–106).

Ramos, V. A., Jordan, T. E., Allmendinger, R. W., Mpodozis, C., Kay, S. M., Cortés, J. M., & Palma, M. (1986). Paleozoic terranes of the central Argentine-Chilean Andes. *Tectonics*, *5*(6), 855–880.

Ramos, V. A., & Kay, S. M. (2006). Overview of the tectonic evolution of the southern Central Andes of Mendoza and Neuquén (35°–39°S latitude). In S. M. Kay & V. A. Ramos (Eds.), *Evolution of an Andean margin: A tectonic and magmatic view from the Andes to the Neuquén Basin (35°–39°S latitude)* (Vol. *407*, pp. 1–17). Geological Society of America, Special Paper. https://doi.org/10.1130/2006.2407(01

Ramos, V. A., Zapata, T., Cristallini, E., & Introcaso, A. (2004). The Andean thrust system—Latitudinal variations in structural styles and orogenic shortening. In K. R. McClay (Ed.), *Thrust tectonics and hydrocarbon system* (Vol. *82*, pp. 30–50). American Association of Petroleum Geologists, Memoir.

Ranero, C. R., von Huene, R., Weinrebe, W., & Reichert, C. (2006). Tectonic processes along the Chile convergent margin. In O. Oncken (Ed.), *The Andes* (pp. 91–121). Springer.

Rapela, C. W., Pankhurst, R. J., Casquet, C., Baldo, E., Galindo, C., Fanning, C. M., & Dahlquist, J. M. (2010). The Western Sierras Pampeanas: Protracted Grenville-age history (1330–1030 Ma) of intra-oceanic arcs, subduction–accretion at continental-edge and AMCG intraplate magmatism. *Journal of South American Earth Sciences*, *29*(1), 105–127.

Rapela, C. W., Pankhurst, R. J., Fanning, C. M., & Herve, F. (2005). Pacific subduction coeval with the Karoo mantle plume: The Early Jurasssic Subcordilleran belt of northwestern Patagonia. *Geological Society of London, Special Publications*, *246*(1), 217–239.

Rapela, C. W., Verdecchia, S. O., Casquet, C., Pankhurst, R. J., Baldo, E. G., Galindo, C., Murra, J. A., Dahlquist, J. A., & Fanning, C. M. (2016). Identifying Laurentian and SW Gondwana sources in the Neoproterozoic to Early Paleozoic metasedimentary rocks of the Sierras Pampeanas: Paleogeographic and tectonic implications. *Gondwana Research*, *32*, 193–212.

Resentini, A., Goren, L., Castelltort, S., & Garzanti, E. (2017). Partitioning sediment flux by provenance and tracing erosion patterns in Taiwan. *Journal of Geophysical Research: Earth Surface*, *122*(7), 1430–1454.

Reynolds, J. H., Jordan, T. E., Johnson, N. M., Damanti, J. F., & Tabbutt, K. D. (1990). Neogene deformation of the flat-subduction segment of the Argentine-Chilean Andes: Magnetostratigraphic constraints from Las Juntas, La Rioja province, Argentina. *Geological Society of America Bulletin*, *102*(12), 1607–1622. https://doi.org/10.1130/0016-7606(1990)102<1607:NDOTFS>2.3.CO;2

Ricci Lucchi, F. (1986). The Oligocene to Recent foreland basins of the northern Apennines. In P. A. Allen & P. Homewood (Eds.), *Foreland basins* (Vol. *8*, pp. 105–139). Blackwell, Oxford, International Association of Sedimentologists, Special Pubblication.

Richetti, P. C., Schmitt, R. S., & Reeves, C. (2018). Dividing the South American continent to fit a Gondwana reconstruction: A model based on continental geology. *Tectonophysics*, *747*, 79–98. https://doi.org/10.1016/j.tecto.2018.09.011

Sato, A. M., Llambías, E. J., Basei, M. A., & Castro, C. E. (2015). Three stages in the Late Paleozoic to Triassic magmatism of southwestern Gondwana, and the relationships with the volcanogenic events in coeval basins. *Journal of South American Earth Sciences*, *63*, 48–69. https://doi.org/10.1016/j.jsames.2015.07.005

Schenk, C. J., Viger, R. J., & Anderson, C. P. (1999). *South America Geologic Map (geo6ag). Maps showing geology, oil and gas fields, and geological provinces of South America region (No. 97-470-D)*. U.S. Geological Survey, Central Energy Resources Team.

Siame, L. L., Bellier, O., Sébrier, M., & Araujo, M. (2005). Deformation partitioning in flat subduction setting: Case of the Andean foreland of western Argentina (28°S–33°S). *Tectonics*, *24*(5), TC5003. https://doi.org/10.1029/2005TC001787

Sinclair, H. D. (1997). Tectonostratigraphic model for underfilled peripheral foreland basins: An Alpine perspective. *Geological Society of America Bulletin*, *109*(3), 324–346.

Sinclair, H. D., & Naylor, M. (2011). Foreland basin subsidence driven by topographic growth versus plate subduction. *Geological Society of America Bulletin*, *124*(3–4), 368–379.

Sinha, R., & Friend, P. F. (1994). River systems and their sediment flux, Indo-Gangetic plains, Northern Bihar, India. *Sedimentology*, *41*(4), 825–845. https://doi.org/10.1111/j.1365-3091.1994.tb01426.x

Søager, N., Holm, P. M., & Llambías, E. J. (2013). Payenia volcanic province, southern Mendoza, Argentina: OIB mantle upwelling in a backarc environment. *Chemical Geology*, *349*, 36–53. https://doi.org/10.1016/j.chemgeo.2013.04.007

Spalletti, L. A., & Isla, F. I. (2003). Características y evolución del delta del Río Colorado ("Colú-Leuvú"), provincia de Buenos Aires, República Argentina. *Latin American Journal of Sedimentology and Basin Analysis*, *10*(1), 23–37.

Stern, C. R. (2004). Active Andean volcanism: Its geologic and tectonic setting. *Revista Geológica De Chile*, *31*(2), 161–206.

Stern, C. R. (2020). The role of subduction erosion in the generation of Andean and other convergent plate boundary arc magmas, the continental crust and mantle. *Gondwana Research*, *88*, 220–249.

Teruggi, M., Chaar, E., Remiro, J., & Limousin, T. (1959). *Las arenas de la costa de la provincia de Buenos Aires entre Cabo San Antonio y Bahía Blanca* (Vol. *12*, pp. 1–77). Provincia de Buenos Aires, Ministerio de Obras Publicas, Laboratorio de Ensayo de Materiales e Investigaciones Tecnológicas, La Plata.

Teruggi, M. E., Etchichury, M., & Remiro, J. (1964). *Las arenas de la costa de la provincia de Buenos Aires entre Bahía Blanca y Río Negro* (Serie II, Vol. *81*, pp. 1–38). Provincia de Buenos Aires, Ministerio de Obras Publicas, Laboratorio de Ensayo de Materiales e Investigaciones Tecnológicas, La Plata.

Thomas, W. A., Astini, R. A., Mueller, P. A., & McClelland, W. C. (2015). Detrital-zircon geochronology and provenance of the Ocloyic synorogenic clastic wedge, and Ordovician accretion of the Argentine Precordillera terrane. *Geosphere*, *11*(6), 1749–1769. https://doi.org/10.1130/GES01212.1

Tripaldi, A., Ciccioli, P. L., Alonso, M. S., & Forman, S. L. (2010). Petrography and geochemistry of late Quaternary dune fields of western Argentina: Provenance of aeolian materials in southern South America. *Aeolian Research*, *2*(1), 33–48. https://doi.org/10.1016/j.aeolia.2010.01.001

Tripaldi, A., & Forman, S. L. (2007). Geomorphology and chronology of Late Quaternary dune fields of western Argentina. *Palaeogeography, Palaeoclimatology, Palaeoecology*, *251*(2), 300–320. https://doi.org/10.1016/j.palaeo.2007.04.007

Tripaldi, A., & Forman, S. L. (2016). Eolian depositional phases during the past 50 ka and inferred climate variability for the Pampean Sand Sea, western Pampas, Argentina. *Quaternary Science Reviews*, *139*, 77–93.

Val, P., Venerdini, A. L., Ouimet, W., Alvarado, P., & Hoke, G. D. (2018). Tectonic control of erosion in the southern Central Andes. *Earth and Planetary Science Letters*, *482*, 160–170. https://doi.org/10.1016/j.epsl.2017.11.004

Valcarce, G. Z., Zapata, T., del Pino, D., & Ansa, A. (2006). Structural evolution and magmatic characteristics of the Agrio fold-and-thrust belt. In S. M. Kay & V. A. Ramos (Eds.), *Evolution of an Andean margin: A tectonic and magmatic view from the Andes to the Neuquén Basin (35°–39°S lat)* (Vol. *407*, pp. 125–146). Geological Society of America, Special Paper.

Vauchel, P., Santini, W., Guyot, J. L., Moquet, J. S., Martinez, J. M., Espinoza, J. C., Baby, P., Fuertes, O., Noriega, L., Puita, O., Sondag, F., Fraizy, P., Armijos, E., Cochonneau, G., Timouk, F., de Oliveira, E., Filizola, N., Molina, J., & Ronchail, J. (2017). A reassessment of the suspended sediment load in the Madeira River basin from the Andes of Peru and Bolivia to the Amazon River in Brazil, based on 10 years of data from the HYBAM monitoring programme. *Journal of Hydrology*, *553*, 35–48.

Vergara Dal Pont, I. P., Caselli, A. T., Moreiras, S. M., & Lauro, C. (2017). Recent coastal geomorphological evolution in the Negro River's mouth (41°S), Argentinean Patagonia. *Journal of Coastal Research*, *33*(6), 1367–1375.

Vergara, I., Moreiras, S. M., Araneo, D., & Garreaud, R. (2020). Geoclimatic hazards in the eastern subtropical Andes: Distribution, climate drivers and trends. *Natural Hazards and Earth System Sciences*, *20*, 1353–1367.

Vezzoli, G., Garzanti, E., Limonta, M., Andó, S., & Yang, S. (2016). Erosion patterns in the Changjiang (Yangtze River) catchment revealed by bulk-sample versus single-mineral provenance budgets. *Geomorphology*, *261*, 177–192.

Violante, R. A., & Parker, G. (2004). The post-last glacial maximum transgression in the de la Plata River and adjacent inner continental shelf. *Argentina. Quaternary International*, *114*(1), 167–181. https://doi.org/10.1016/S1040-6182(03)00036-3

Vogt, H., Vogt, T., & Calmels, A. P. (2010). Influence of the post-Miocene tectonic activity on the geomorphology between Andes and Pampa Deprimida in the area of Provincia de La Pampa, Argentina. *Geomorphology*, *121*, 152–166. https://doi.org/10.1016/j.geomorph.2010.03.011

von Gosen, W. (1992). Structural evolution of the argentine precordillera: The Río San Juan section. *Journal of Structural Geology*, *14*(6), 643–667.

von Huene, R., Corvalán, J., Flueh, E. R., Hinz, K., Korstgard, J., Ranero, C. R., & Weinrebe, W. (1997). Tectonic control of the subducting Juan Fernández Ridge on the Andean margin near Valparaiso, Chile. *Tectonics*, *16*(3), 474–488. https://doi.org/10.1029/96TC03703

Yáñez, G. A., Ranero, C. R., von Huene, R., & Díaz, J. (2001). Magnetic anomaly interpretation across the southern central Andes (32–34°S): The role of the Juan Fernández Ridge in the late Tertiary evolution of the margin. *Journal of Geophysical Research: Solid Earth*, *106*(B4), 6325–6345.

Zapata, T., & Folguera, A. (2005). Tectonic evolution of the Andean fold and thrust belt of the southern Neuquén Basin, Argentina. *Geological Society of London, Special Publications*, *252*(1), 37–56. https://doi.org/10.1144/GSL.SP.2005.252.01.03

Zárate, M., & Blasi, A. (1993). Late Pleistocene-Holocene eolian deposits of the southern Buenos Aires Province, Argentina:

A preliminary model. *Quaternary International*, *17*, 15–20. https://doi.org/10.1016/1040-6182(93)90075-Q

Zárate, M. A., & Tripaldi, A. (2012). The aeolian system of central Argentina. *Aeolian Research*, *3*(4), 401–417. https://doi.org/10.1016/j.aeolia.2011.08.002

SUPPORTING INFORMATION

Additional Supporting Information may be found online in the Supporting Information section.

How to cite this article: Garzanti, E., Capaldi, T., Vezzoli, G., Limonta, M., & Sosa, N. (2021). Transcontinental retroarc sediment routing controlled by subduction geometry and climate change (Central and Southern Andes, Argentina). *Basin Research*, 33, 3406–3437. https://doi.org/10.1111/bre.12607